# Free-Space Optical Communications: Capacity Bounds, Approximations, and a New Sphere-Packing Perspective

Anas Chaaban, Jean-Marie Morvan, and Mohammad Slim Alouini

**Abstract**

The capacity of the intensity-modulation direct-detection (IM-DD) free-space optical channel is studied. A new recursive approach for bounding the capacity of the channel based on sphere-packing is proposed, which leads to a tighter bound than an existing sphere-packing bound for the channel with only an average intensity constraint. Under both average and peak constraints, it yields bounds that characterize the high SNR capacity within a negligible gap, where the achievability is proved by using a truncated-Gaussian input distribution. Simple fitting functions that capture the best known achievable rate for the channel are provided. These functions can be of significant practical importance especially for the study of systems operating under atmospheric turbulence and misalignment conditions. Finally, the capacity/SNR loss between heterodyne detection (HD) systems and IM-DD systems is bounded at high SNR, where it is shown that the loss grows as SNR increases for a complex-valued HD system, while it is bounded by $1.745$ bits or $5.26$ dB at most for a real-valued one. This comparison relies on a newly proposed cost-dependent channel model, which has input independent noise, but still takes into account the increasing impact of shot-noise at high SNR.

**Index Terms**

Intensity-modulation, sphere-packing, capacity bounds, capacity approximation, truncated-Gaussian.

## I. Introduction

Free-space optical (FSO) communication has attracted lots of research attention recently [1]–[6] due to its ability to provide high-speed communication while not being too demanding in terms of infrastructure [7], [8]. As such, it is an important solution for scenarios where deploying infrastructure is either prohibitive (dangerous terrain) or not cost-effective (temporary situations).

Studying the capacity of Intensity-Modulation Direct-Detection (IM-DD) systems has attracted lots of research attention recently [9]–[11]. This attention is driven by the increasing interest in IM-DD especially for optical wireless

Parts of this paper have been presented in IWOW'2015.

The authors are with the Division of Computer, Electrical, and Mathematical Sciences and Engineering (CEMSE) at King Abdullah University of Science and Technology (KAUST), Thuwal, Saudi Arabia. Email: {anas.chaaban,jean-marie.morvan,slim.alouini}@kaust.edu.sa.

J.-M. Morvan is on leave from Université de Lyon, CNRS, Université Claude Bernard Lyon 1, ICJ UMR 5208, Villeurbanne F-69622 France.

This work is supported in part by King Abdulaziz City of Science and Technology (KACST) under grant AT-34-145.

communications (OWC) [1]–[3], [12]. The interest in OWC is due to its ability to provide high-speed communication while not being too demanding in terms of infrastructure [7], [8]. As such, it is an important solution for scenarios where deploying infrastructure is either prohibitive (dangerous terrain) or not cost-effective (temporary situations). OWC is also a potential solution for one the main problems facing today's radio-frequency (RF) communication: spectrum shortage.

Although optical heterodyne detection (HD) enables quadrature and amplitude modulation [13], IM-DD is favored from a practical point of view due to its simplicity and low-cost. Several models exist for IM-DD channels [7], and one of the most often studied models is the Gaussian channel with input-independent Gaussian noise [9]–[11], [14]. In this model, the input signal is a positive random variable representing the optical intensity, and the noise is input-independent Gaussian. In addition to its non-negativity, the input signal is typically restricted by a peak and an average constraint due to safety and practical considerations [15]. Although the capacity achieving input distribution is known to be a discrete [14], the capacity of the channel is yet unknown in closed-form.

Nevertheless, several upper and lower bounds exist on the channel capacity, and these bounds are close in some cases. For instance, for the channel with an average constraint only, [9] derived capacity upper and lower bounds that meet at high signal-to-noise ratio (SNR). Under an average and peak intensity constraints, the upper and lower bounds in [9] meet at high and low SNR. The highest known achievable rate for the channel was given in [10], where the best discrete distribution with equally spaced mass points was found. This distribution is close to optimal as shown in [10]. On the other hand, [11] derived bounds for the channel under an average constraint only, where it was shown that the best discrete distribution with equally spaced mass points is the geometric distribution. In the same paper, an upper bound was derived by interpreting the problem of capacity characterization as a problem of packing spheres in a simplex. Despite this work, a simple capacity expression is still to be found.

### *A. Contributions*

Our work in this paper can be considered rather complementing the work in [9], [10] for an IM-DD channel with both average and peak constraints. Let us first summarize the contributions before discussing them one by one.

1) We propose a new approach for deriving sphere-packing bounds for channels with peak or average intensity constraints. These bounds are fairly tight for moderate/high SNR. We also show that our approach yields a tighter bound than the sphere-packing bound given in [11] for any SNR.
2) We provide a simple alternative derivation of an upper bound given in [9].
3) We derive the rate achievable by using a truncated-Gaussian (TG) input distribution, and show that it is nearly optimal at high SNR.
4) We provide simple fitting functions that capture the best known achievable rate of the channel given in [10].
5) For an IM-DD channel with input-dependent noise as in [16], we show that the capacity of the input-dependent channel is lower bounded at high SNR by the capacity of a channel with input-independent Gaussian noise whose variance depends on the input cost. Based on this, we propose an IM-DD cost-dependent Gaussian channel model for OWC.
6) We derive bounds on capacity/SNR loss between HD systems and IM-DD systems at high SNR.

Now we briefly discuss these contributions. Similar to [11], we interpret the capacity characterization of the IM-DD channel as a problem of sphere-packing. Under a peak constraint, we get a problem of sphere-packing in a cube. We derive upper bounds for this case using two approaches. The first approach is similar to the one used in [11] which employs the Steiner-Minkowski formula for polytopes [17]–[19]. This approach is 'almost' independent of the geometry of the sphere in the sense that replacing the sphere by any other shape (or even a liquid) with the same volume yields the same bound. Then, we propose a new approach based on a recursive argument. The new approach is geometry-dependent, and yields better bounds at moderate/high SNR. For the IM-DD channel with only an average constraint, applying our approach to sphere-packing in a simplex yields a significantly better bound than the one derived in [11] for any SNR. This is clearly due to exploiting the geometry of the sphere while deriving the bounds. The derived sphere-packing bounds coincide with the high SNR capacity of the channel with an average constraint only, and the channel with average and peak constraints with a dominant peak constraint, and thus, reproduce the result of [9]. The advantage is that sphere-packing bounds have a simpler interpretation than the bounds in [9] due to their geometric nature.

In [9], continuous input distributions were given that achieve the high SNR capacity of the channel. We ask the questions whether other continuous distributions can achieve higher rates at moderate SNR. To this end, we derive the rate achievable by using a TG input distribution. This achievable rate answers this question in the affirmative. The expression of the achievable rate is rather complicated in general, and requires optimization over two parameters. We provide a lower bound on this achievable rate which has a simpler expression. We also provide values for the optimization parameters which yield a fairly good performance at high SNR. In particular, we show that the TG distribution is nearly capacity achieving at high SNR if the peak constraint dominates the average constraint. Otherwise, if the average constraint dominates, we show that the TG distribution achieves the sphere-packing bounds within a gap of at most $0.163$ nats, although this gap can be reduced numerically to $0.1$ nats. Based on this result, we approximate the capacity by the sphere-packing bounds at high SNR. We note that the gap reduces to approximately zero by incorporating a bound from [9]. This leads to the conclusion that the TG distribution is nearly capacity achieving at high SNR.

The best achievable rate known to-date is the one given in [10], which is sufficiently close to the upper bounds at any SNR. However, this achievable rate is derived numerically, and does not have a closed-form expression. Such a closed-form expression is important for the study of the performance of practical systems under fading scenarios. The availability of such an expression allows a better understanding of the ultimate performance of IM-DD systems beyond simple sub-optimal schemes such as on-off keying [1], [2], [12] or binary pulse-position modulation [20], [21], and beyond high SNR scenarios with only an average constraint [22]. To make the capacity approaching scheme in [10] more accessible, we provide a simple fitting function which closely captures its achievable rate globally (at any SNR). This expression is of the form $\frac{1}{2}\log(1+\gamma^2 f(\gamma))$ where $\gamma$ is the SNR and $f(\gamma)$ is of the form $p(\gamma)/q(\gamma)$ which are both polynomials of the same degree in $\gamma$. It turns out that fixing the degrees of these polynomials to 1 provides a sufficiently good fit, while increasing it to 3 provides a very close fit at the expense of a more sophisticated expression. We also provide a rather simpler fitting function of the form $\frac{d_1}{2}\log(1+d_3\gamma^2)$ which provides a close fit locally within a desired range of SNR.

The aforementioned results apply to a channel with input-independent noise. However, the IM-DD channel has noise which is dependent on the input in general [16]. Using the input-independent Gaussian IM-DD channel model from [9] is accurate at low SNR, however, it loses its accuracy at high SNR where shot-noise dominates, and the noise becomes input-dependent. This can be seen by comparing results on both models at high SNR [16]. Nevertheless, dealing with an input-independent Gaussian IM-DD is more convenient. Thus, it is interesting to find an input-independent channel model, which better captures the high SNR performance of the channel. We prove a lemma leading to such a model. Namely, we show that for an IM-DD channel with input-dependent noise, the high-SNR capacity is lower bounded by the capacity of an IM-DD channel with input-independent noise whose variance depends on the input cost. This leads to the our *cost-dependent Gaussian IM-DD channel model* where the noise variance depends on the average and peak constraints. Results for IM-DD channels with input-independent noise [9]–[11], [14] apply to this model. The dependence of the noise in this model on the input cost leads high SNR capacity scaling which matches [16].

Finally, we investigate the capacity/SNR loss between HD and IM-DD at high SNR. The comparison is performed under the same optical intensity constraints. For HD, the SNR is strongly dependent on the power of the optical local oscillator (LO) [13]. To guarantee a fair comparison between HD and IM-DD, this dependence on the LO power has to be eliminated, which is possible under shot-noise dominated operation with sufficiently high LO power. However, a shot-noise dominated IM-DD channel has input-dependent noise variance. We lower bound the high-SNR capacity of an input-dependent IM-DD by that of a cost-dependent IM-DD. We apply the high SNR results to bound the gap between HD and IM-DD. While the gap grows as a function of SNR for a complex-valued HD system, it can be bounded by $1.745$ bits or equivalently $5.26$ dB for real-valued HD systems (this is to be made more precise in the sequel). This provides a benchmark for choosing between HD or IM-DD based on their capacity gap and different cost and complexity.

### *B. Organization*

The rest of the paper is organized as follows. The system model is given in Section II. The main results of the paper are given in Section III, and are proved in the remaining sections. Namely, in Section IV, we derive upper bounds for sphere-packing in a cube using the Steiner-Minkowski approach used in [11] and our recursive approach, and we compare the resulting bounds. In Section V, we use our recursive approach to derive an upper bound for sphere-packing in a simplex. In Section VI, we derive the achievable rate using a TG distribution, and approximate the high-SNR capacity. We provide capacity fitting functions in Section VII and compare HD and IM-DD in Section VIII. Finally, we conclude in Section IX.

### *C. Notation*

Throughout the paper, we use normal-face font to denote scalars, and bold-face font to denote vectors. We use $X \sim g_{\mu,\sigma}(x)$ to indicate that $X$ is Gaussian distributed with mean $\mu$ and variance $\sigma^2$, and we use $G_{\mu,\sigma}(x)$ to denote the corresponding cumulative distribution function. We denote the variance of a random variable $X$ by $\mathrm{Var}(X)$.

We also use $V(\cdot)$ to denote the volume of an object, and $A(\cdot)$ to denote its surface area. Next, we introduce the IM-DD channel.

## II. The Intensity-Modulation Direct-Detection Channel

We consider an IM-DD channel whose input $X > 0$ is a random variable representing the intensity of the optical signal. Since intensity is constrained due to practical and safety restrictions by average and peak constraints in general [15], the input random variable has to satisfy $X \leq \mathcal{A}$ and $\mathbb{E}[X] \leq \mathcal{E}$.

To send a message $w \in \{1, \cdots, M\}$ to the destination, the source encodes it into a codeword $\mathbf{X}(w) = (X_1(w), \cdots, X_n(w))$ of length $n$ symbols, and sends this codeword over the channel. Here, the symbols $X_i(w)$ are realizations of the random variable $X$. An intensity detector is used at the destination to detect $\mathbf{X}(w)$. The received signal after the detector is $\mathbf{Y} = \mathbf{X} + \mathbf{Z}$ where $\mathbf{Z}$ is a sequence of $n$ independent and identically distributed $Z \sim g_{0,\sigma}(z)$, independent of $X$. Throughout the paper, we denote the peak signal-to-noise ratio (PSNR) $\frac{\mathcal{A}}{\sigma}$ by $\gamma$, and the average signal-to-noise ratio (ASNR) $\frac{\mathcal{E}}{\sigma}$ by $\bar{\gamma}$. In general, we say that the IM-DD has high SNR if $\bar{\gamma} \gg 1$, which for a given APR $\frac{\mathcal{E}}{\mathcal{A}}$, implies that $\gamma \gg 1$.

The destination uses a decoder to recover $\hat{w} \in \{1, \cdots, M\}$ from the received signal $\mathbf{Y}$. An error occurs if $\hat{w} \neq w$, and has a probability $P_e^{(n)}$. The goal of the paper is to bound the capacity $\mathcal{C}$ of transmission over the given IM-DD channel (in units of nats per channel use). The capacity is the maximum achievable transmission rate. The transmission rate in turn is defined as $R = \frac{\log(M)}{n}$, where $R$ is said to be achievable if the error probability of the transmission $P_e^{(n)}$ can be made arbitrarily small $P_e^{(n)} \to 0$ by letting $n \to \infty$.

The capacity of the channel can be expressed as $\mathcal{C} = \max_{f(x) \in \mathcal{F}} I(X;Y)$ [23], where $f(x)$ is a distribution of $X$ and $\mathcal{F}$ is the set of distributions of $X \in [0, \mathcal{A}]$ satisfying $\mathbb{E}[X] \leq \mathcal{E}$. Although it is known that the capacity achieving distribution of such a channel is discrete [14], this distribution is yet unknown explicitly. The main goal of this work is to study the capacity of the channel, and to provide simple approximations of this capacity that can be useful in practice.

## III. Main Results

We first present a simple result on the optimal $\mathbb{E}[X]$ as given in the following lemma.

*Lemma 1:* In an input-independent Gaussian IM-DD channel, the optimal distribution of $X$ satisfies $\mathbb{E}[X] = \min\left\{\mathcal{E}, \frac{\mathcal{A}}{2}\right\}$.

*Proof:* The proof is given in Appendix A. ■

Note that this generalizes the result in [9, Proposition 9] stating that the capacity of an input-independent Gaussian noise IM-DD channel admits a maximum at $\mathbb{E}[X] = \frac{\mathcal{A}}{2}$.

The next results concerns the IM-DD channel with a peak constraint only.

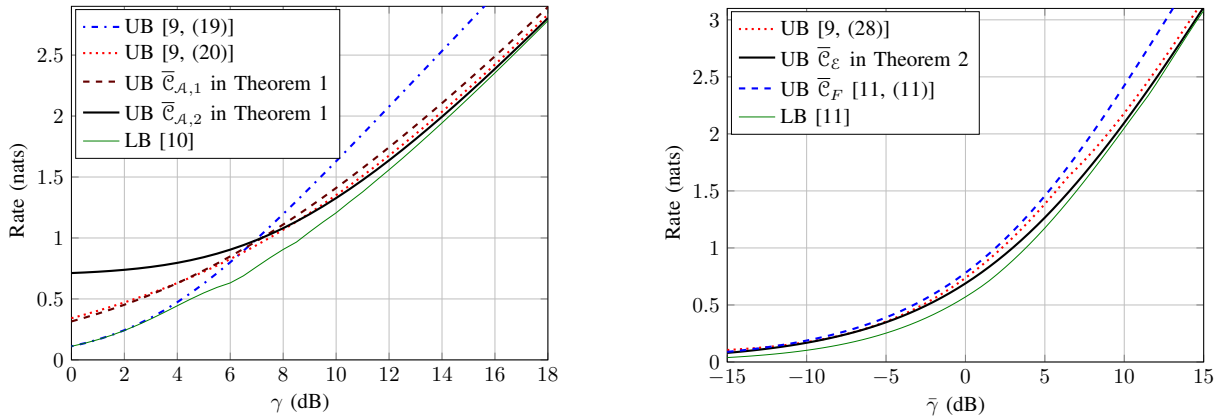


(a) Peak only.

(b) Average only.

Fig. 1: A comparison between different capacity upper bounds (UB) and the best known lower bound (LB) for an IM-DD channel with either a peak constraint of an average constraint.

*Theorem 1:* The capacity $\mathcal{C}_{\mathcal{A}}$ of an IM-DD channel with a peak constraint only satisfies $\mathcal{C}_{\mathcal{A}} \leq \overline{\mathcal{C}}_{\mathcal{A},i}$, $i \in \{1,2\}$, where $\overline{\mathcal{C}}_{\mathcal{A},i} = \sup_{\alpha\in[0,1]} B_i(\alpha)$ and

$$B_1(\alpha) = \alpha \log\left(\frac{\gamma}{\sqrt{2\pi e}}\right) - \log\left(\alpha^{\alpha}(1-\alpha)^{\frac{3(1-\alpha)}{2}}\right) \tag{1}$$

$$B_2(\alpha) = \alpha \log\left(\frac{\gamma}{\sqrt{2\pi e}}\right) - \log\left(\alpha^{\frac{\alpha}{2}}(1-\alpha)^{1-\alpha}2^{\alpha-1}\right). \tag{2}$$

*Proof:* The proof is given in Section IV. ■

Those bounds are derived using sphere-packing arguments. In particular, to bound the capacity, we bound the number of spheres that can be packed so that their centers are located within a cube of side-length $\mathcal{A}$. This problem can be approached by using the Steiner-Minkowski formula leading to $\overline{\mathcal{C}}_{\mathcal{A},1}$. In addition to this approach, we propose a new approach based on a recursive argument which leads to $\overline{\mathcal{C}}_{\mathcal{A},2}$. The main idea of the recursive approach is bounding the number of spheres (and portions thereof) inside an $n$-dimensional cube, then inside its $(n-1)$-dimensional faces which are $(n-1)$-dimensional cubes, and so on until the 0-dimensional faces which are the vertices of the cube.

Fig. 1a shows several capacity upper bounds as a function of the PSNR $\gamma$ for a channel with a peak constraint *only*. Here we can see that the upper bound $\overline{\mathcal{C}}_{\mathcal{A},2}$ is the tightest at moderate/high PSNR ($\gamma > 8$ dB) and that it converges faster to the high PSNR capacity of the channel. For comparison, the best known lower bound given in [10] is shown. This lower bound is achievable by using a discrete uniform input distribution with equally spaced mass points, i.e., by solving $\max_{K\geq 2} I(X;Y)$ where $X$ follows the distribution $f(x) = \sum_{k=0}^{K} \frac{1}{K+1}\delta(x-k\ell)$, $\ell = \mathcal{A}/K$, and $\delta(\cdot)$ is the Dirac delta function. The bounds [9, (19)] and $\overline{\mathcal{C}}_{\mathcal{A},2}$ provide a tight capacity characterization at low and high PSNR, respectively.

Under an average constraint only, we have the following bound.

*Theorem 2:* The capacity $\mathcal{C}_{\mathcal{E}}$ of an IM-DD channel with an average constraint only satisfies $\mathcal{C}_{\mathcal{E}} \leq \overline{\mathcal{C}}_{\mathcal{E}}$ where $\overline{\mathcal{C}}_{\mathcal{E}} = \sup_{\alpha\in[0,1]} B_3(\alpha)$, and

$$B_3(\alpha) = \alpha \log\left(\frac{\sqrt{e}\bar{\gamma}}{\sqrt{2\pi}}\right) - \log\left((1-\alpha)^{1-\alpha}\alpha^{\frac{3\alpha}{2}}\right). \tag{3}$$

*Proof:* The proof is given in Section V. ■

This bound is derived using a sphere-packing interpretation. In particular, $\overline{\mathcal{C}}_{\mathcal{E}}$ is obtained by upper bounding the number of spheres that can be packed in a simplex. It is derived using the recursive approach. The approach using the Steiner-Minkowski formula yields the bound [11] $\mathcal{C}_{\mathcal{E}} \leq \overline{\mathcal{C}}_F = \sup_{\alpha\in[0,1]} B_4(\alpha)$ where

$$B_4(\alpha) = B_3(\alpha) + \frac{\alpha}{2}\log\left(\frac{e}{2}\right) - \frac{1}{2}\log\left(\frac{(1-\frac{\alpha}{2})^{2-\alpha}}{(1-\alpha)^{1-\alpha}}\right).$$

By direct comparison, it can be shown that $B_3(\alpha) \leq B_4(\alpha)$ for all $\alpha \in [0,1]$ with equality if $\alpha = 0$. Our upper bound is tighter because it exploits the geometry of the ball as we shall see in Section V. Our bound $\overline{\mathcal{C}}_{\mathcal{E}}$ coincides at high ASNR with the capacity of the channel with an average constraint *only* given in [9, Proposition 8], but has a simpler expression. Fig. 1b shows several upper bounds as a function of ASNR $\bar{\gamma}$. It can be seen that our bound $\overline{\mathcal{C}}_{\mathcal{E}}$ is closest to the best known lower bound given in [11]. This lower bound is achieved by using a discrete geometric input distribution with equally spaced mass points, i.e., by solving $\max_{\ell>0} I(X;Y)$ where $X$ follows the distribution $f(x) = \sum_{k=0}^{\infty} \frac{\ell}{\ell+\mathcal{E}}\left(\frac{\mathcal{E}}{\ell+\mathcal{E}}\right)^k \delta(x-k\ell)$.

Since dropping a constraint does not decrease capacity, the capacity of the IM-DD channel with both average and peak constraints is upper bounded by that of a channel with one constraint only, leading to the following corollary.

*Corollary 1:* The capacity $\mathcal{C}$ of an IM-DD channel with an average constraint $\mathcal{E}$ and a peak constraint $\mathcal{A}$ is upper bounded by $\overline{\mathcal{C}}_{\mathcal{E}}$, $\overline{\mathcal{C}}_{\mathcal{A},1}$, and $\overline{\mathcal{C}}_{\mathcal{A},2}$.

The bounds $\overline{\mathcal{C}}_{\mathcal{A},1}$ and $\overline{\mathcal{C}}_{\mathcal{A},2}$ are tight at high SNR if $\frac{\mathcal{E}}{\mathcal{A}} \geq \frac{1}{2}$ which reproduces [9, Corollary 6], but are simpler and more intuitive than the bounds in [9]. As we shall show, the upper bound $\overline{\mathcal{C}}_{\mathcal{E}}$ is fairly tight at high SNR if $\frac{\mathcal{E}}{\mathcal{A}} < \frac{1}{2}$.

A tight upper bound for this case was given in [9, (11) & (19)]. This upper bound is given as follows.

*Theorem 3 ( [9, (11) & (19)]):* The capacity $\mathcal{C}$ satisfies $\mathcal{C} \leq \overline{\mathcal{C}}$ where $\overline{\mathcal{C}} = \frac{1}{2}\log\left(1+\frac{\gamma^2}{4}\right)$ if $\frac{\mathcal{E}}{\mathcal{A}} \geq \frac{1}{2}$ and $\overline{\mathcal{C}} = \frac{1}{2}\log\left(1+\bar{\gamma}(\gamma-\bar{\gamma})\right)$ otherwise.

*Proof:* This bound was derived in [9] using a duality approach. An alternative proof of this theorem is given in Section VI-A. ■

We derive the achievable rate of the truncated-Gaussian (TG) distribution satisfying both average and peak constraints, as given in the following theorem.

*Theorem 4:* The capacity $\mathcal{C}$ satisfies $\mathcal{C} \geq \mathcal{R} \geq \mathcal{R}'$ where the achievable rates $\mathcal{R}$ and $\mathcal{R}'$ are given by $\mathcal{R} = \mathcal{R}' - \Phi_3(\mu,\nu)$ and $\mathcal{R}' = \mathcal{C}_0(\nu) - \Phi_1(\mu,\nu) - \Phi_2(\mu,\nu)$, and where $\mathcal{C}_0(\nu) = \frac{1}{2}\log\left(1+\frac{\nu^2}{\sigma^2}\right)$, $\Phi_1(\mu,\nu) = \log(\eta)$,

$$\Phi_2(\mu,\nu) = \left((\mathcal{A}-\mu)g_{\mu,\nu}(\mathcal{A}) + \mu g_{\mu,\nu}(0)\right)\frac{\eta\nu^2}{2(\nu^2+\sigma^2)}, \tag{4}$$

$$\Phi_3(\mu,\nu) = \mathbb{E}_{X,Y}\left[\log(G_{\mu',\nu'}(\mathcal{A}) - G_{\mu',\nu'}(0))\right], \tag{5}$$

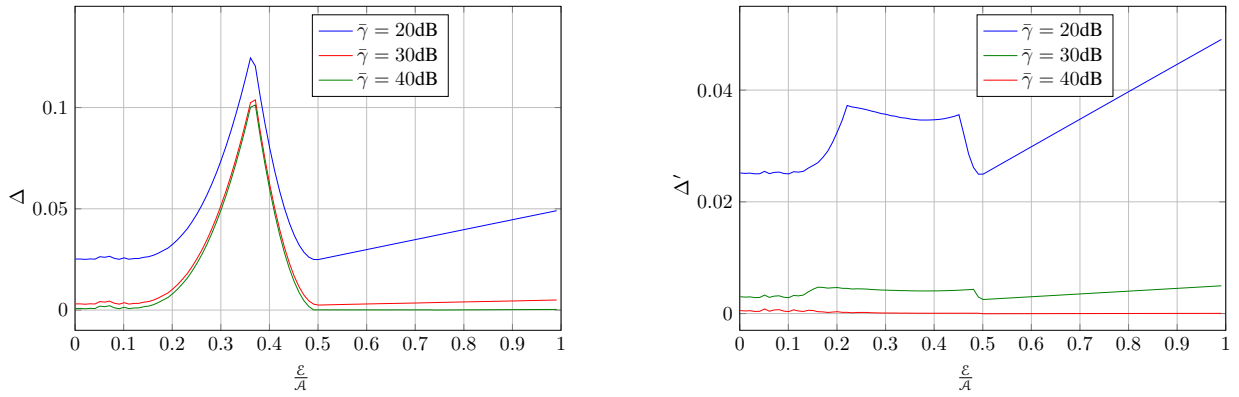


(a) $\Delta = \min\{\overline{\mathcal{C}}_{\mathcal{E}}, \overline{\mathcal{C}}_{\mathcal{A},2}\} - \mathcal{R}'$.

(b) $\Delta' = \min\{\overline{\mathcal{C}}_{\mathcal{E}}, \overline{\mathcal{C}}_{\mathcal{A},2}, \overline{\mathcal{C}}_{L,1}\} - \mathcal{R}'$.

Fig. 2: The gap between the sphere-packing bounds and the truncated-Gaussian lower bound for different ratios $\frac{\mathcal{E}}{\mathcal{A}}$.

for some parameters $\mu$ and $\nu$ satisfying $\nu^2\eta(g_{\mu,\nu}(0) - g_{\mu,\nu}(\mathcal{A})) + \mu \leq \min\{\mathcal{E}, \frac{\mathcal{A}}{2}\}$, with $\eta = (G_{\mu,\nu}(\mathcal{A}) - G_{\mu,\nu}(0))^{-1}$, $\mu' = \frac{\mu\sigma^2 + y\nu^2}{\nu^2+\sigma^2}$, $\nu' = \frac{\nu\sigma}{\sqrt{\nu^2+\sigma^2}}$, and the expectation in $\Phi_3(\mu,\nu)$ is taken with respect to the distribution $f(x,y) = \eta g_{\mu,\nu}(x) g_{x,\sigma}(y)$ over $x \in [0,\mathcal{A}]$ and $y \in \mathbb{R}$.

*Proof:* This theorem is proved in Section VI-B. ■

The achievable rate $\mathcal{R}$ has a sophisticated expression, whereas $\mathcal{R}'$ is rather simpler to compute, and is also simpler than $\mathcal{R}_F$ in [10]. At high SNR, we can show that specific choices of $\mu$ and $\nu$ lead to $\mathcal{R}'$ being close to the sphere-packing bounds. Furthermore, by numerically optimizing with respect to $\mu$ and $\nu$, we observe that $\mathcal{R}'$ is within a gap of 0 and $< 0.1$ nats per channel use at high SNR of the sphere-packing bounds $\overline{\mathcal{C}}_{\mathcal{A},2}$ and $\overline{\mathcal{C}}_{\mathcal{E}}$ for $\frac{\mathcal{E}}{\mathcal{A}} \geq \frac{1}{2}$ and $\frac{\mathcal{E}}{\mathcal{A}} < \frac{1}{2}$, respectively (Fig. 2a). Since the gap between the bounds is negligible at high SNR, we make the following approximation.

*Proposition 1:* The high SNR capacity of a channel with both average and peak constraints can be approximated by $\mathcal{C}_{\text{High SNR}} \approx \min\left\{\frac{1}{2}\log\left(\frac{e\bar{\gamma}^2}{2\pi}\right), \frac{1}{2}\log\left(\frac{\gamma^2}{2\pi e}\right)\right\}$.
These expressions are the limits of $\overline{\mathcal{C}}_{\mathcal{E}}$ and $\overline{\mathcal{C}}_{\mathcal{A},2}$ as $\gamma \to \infty$. The approximation gap is at most 0.1 nats.

*Remark 1:* It can be shown numerically that $\mathcal{R}'$ (and consequently $\mathcal{R}$) is nearly capacity achieving at high SNR. This statement is based on the negligible gap, at high SNR, between $\mathcal{R}'$ and the upper bound given by $\min\{\overline{\mathcal{C}}_{\mathcal{E}}, \overline{\mathcal{C}}_{L,1}, \overline{\mathcal{C}}_{\mathcal{A},2}\}$ with $\overline{\mathcal{C}}_{L,1}$ being the bound given in [9, (12)] (see Fig. 2b).

*Remark 2:* The high-SNR capacity of a channel with both average and peak constraints is within $\approx 0$ and 0.1 nats at most of the sphere-packing bound $\overline{\mathcal{C}}_{\mathcal{E}}$ for $\frac{\mathcal{E}}{\mathcal{A}} \leq 0.15$ and $0.15 < \frac{\mathcal{E}}{\mathcal{A}} \leq \frac{1}{e}$, respectively (see Fig. 2). This bounds is in turn tight at high SNR for a channel with an average constraint only. Therefore, for a channel with an average constraint only, imposing a peak constraint $\mathcal{A} \geq e\mathcal{E}$ or $\mathcal{A} \geq \frac{20}{3}\mathcal{E}$ leads to a high SNR capacity loss of at most 0.1 nats or $\approx 0$, respectively.

The resulting bounds are plotted in Fig. 3. In general, the sphere-packing bounds $\overline{\mathcal{C}}_{\mathcal{E}}$ and $\overline{\mathcal{C}}_{\mathcal{A},2}$ are fairly tight at moderate/high SNR. The bound $\overline{\mathcal{C}}_{\mathcal{E}}$ is tighter than $\overline{\mathcal{C}}_{\mathcal{A},2}$ when the $\frac{\mathcal{E}}{\mathcal{A}}$ is small (thus, we do not plot $\overline{\mathcal{C}}_{\mathcal{A},2}$ in Fig. 3a and 3b). The transition point where $\overline{\mathcal{C}}_{\mathcal{A},2}$ becomes tighter than $\overline{\mathcal{C}}_{\mathcal{E}}$ occurs around $\frac{\mathcal{E}}{\mathcal{A}} = \frac{1}{e}$. At this point,

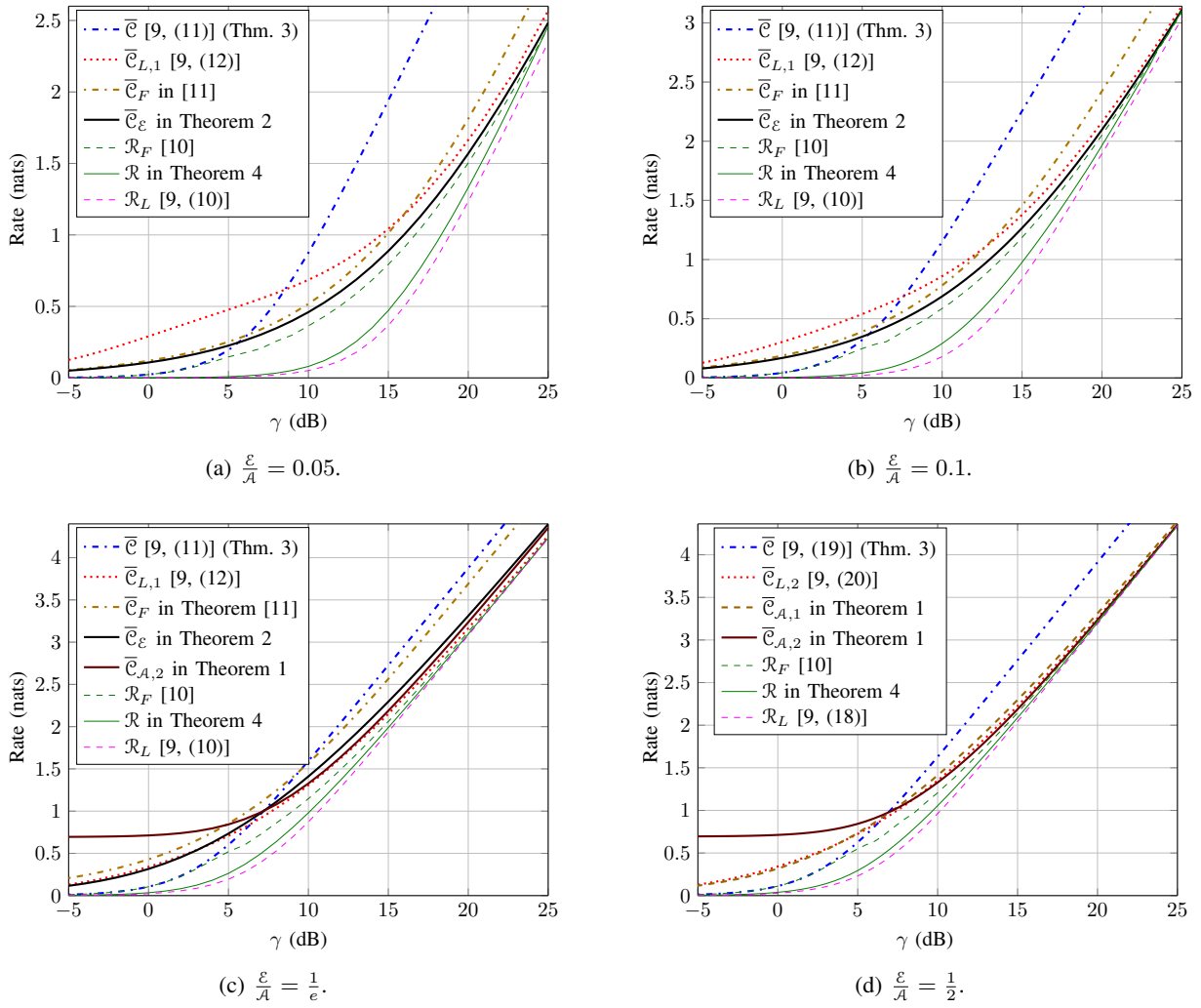


(a) $\frac{\mathcal{E}}{\mathcal{A}} = 0.05$. (b) $\frac{\mathcal{E}}{\mathcal{A}} = 0.1$.

(c) $\frac{\mathcal{E}}{\mathcal{A}} = \frac{1}{e}$. (d) $\frac{\mathcal{E}}{\mathcal{A}} = \frac{1}{2}$.

Fig. 3: The capacity upper bounds and lower bounds plotted versus the signal-to-noise ratio $\gamma$ for several ratios $\frac{\mathcal{E}}{\mathcal{A}}$. Note that $\frac{\mathcal{E}}{\mathcal{A}} = \frac{1}{2}$ represents all scenarios with $\frac{\mathcal{E}}{\mathcal{A}} \geq \frac{1}{2}$ (including the case with only a peak constraint) since they have the same capacity [9].

the bound given in [9, (12)] which we denote $\overline{\mathcal{C}}_{L,1}$, becomes slightly tighter than $\overline{\mathcal{C}}_{\mathcal{A},2}$. The reason is that under both average and peak constraints, the feasible region of the codeword $\mathbf{X}$ is the intersection of a simplex and a cube. This intersection becomes more similar to a simplex at small $\frac{\mathcal{E}}{\mathcal{A}}$, and more similar to a cube at large $\frac{\mathcal{E}}{\mathcal{A}}$. At moderate $\frac{\mathcal{E}}{\mathcal{A}}$, treating this intersection as either a simplex or a cube enlarges the upper bound. In summary, the bounds $\overline{\mathcal{C}}_{\mathcal{E}}$, $\overline{\mathcal{C}}$, $\overline{\mathcal{C}}_{L,1}$, and $\mathcal{R}_F$ provide the tightest capacity bounding for all SNR for $\frac{\mathcal{E}}{\mathcal{A}} < \frac{1}{e}$. On the other hand, the bounds $\overline{\mathcal{C}}_{\mathcal{A},2}$, $\overline{\mathcal{C}}$, $\overline{\mathcal{C}}_{L,2}$ [9, (20)], and $\mathcal{R}_F$ provide the tightest capacity bounding for all SNR for $\frac{\mathcal{E}}{\mathcal{A}} > \frac{1}{e}$.

Simple capacity expressions are of theoretical importance since they can be used to study fading channels [22], [24]. From this point of view, it is interesting to find simple fitting functions which capture the best known achievable

| Case | HD-PAM vs. IM-DD | | HD vs. IM-DD | |
|---|---|---|---|---|
| | Capacity gap (bit) | SNR gap (dB) | Capacity gap (bit) | SNR gap (dB) |
| Peak only or $\alpha > \frac{1}{2}$ | 1.5 | 4.52 | $\log_2\left(\frac{8\gamma}{\sqrt{\pi e}}\right)$ | $10\log_{10}\left(\frac{8\gamma}{\sqrt{\pi e}}\right)$ |
| $\frac{1}{e} < \alpha \leq \frac{1}{2}$ | 1.645 | 4.95 | | |
| $0.15 < \alpha \leq \frac{1}{e}$ | 1.745 | 5.26 | $\log_2\left(\bar{\gamma}\frac{\sqrt{8\pi}}{\sqrt{e}}\right)$ | $10\log_{10}\left(\bar{\gamma}\frac{\sqrt{8\pi}}{\sqrt{e}}\right)$ |
| Average only or $\alpha \leq 0.15$ | 1.6 | 4.83 | | |

TABLE I: Gap between an HD system and an IM-DD system at high SNR. Here, $\gamma = \mathcal{A}/\sigma$ and $\bar{\gamma} = \mathcal{E}/\sigma$. The SNR dependent gaps are expressed with respect to the SNR of the HD system.

rate $\mathcal{R}_F$ given in [10]. It turns out that a globally close fit for $\mathcal{R}_F$ can be obtained by using the function

$$\Psi(\gamma) = \frac{1}{2}\log\left(1 + \gamma^2(c_1 + (c_2 - c_1)\frac{\Theta_1(\gamma)}{\Theta_2(\gamma)})\right),$$

where $c_1 = \min\left\{\frac{e\bar{\gamma}^2}{2\pi\gamma^2}, \frac{1}{2\pi e}\right\}$, $c_2 = \min\left\{\frac{\bar{\gamma}}{\gamma}\left(1 - \frac{\bar{\gamma}}{\gamma}\right), \frac{1}{4}\right\}$, and where $\Theta_1(\gamma)$ and $\Theta_2(\gamma)$ are polynomials of degrees $m_1$ and $m_2 > m_1$ in $\gamma$, respectively. Choosing $(m_1, m_2) = (0, 1)$ gives a good fit, with a slight improvement by choosing $(m_1, m_2) = (1, 2)$. The coefficients of the polynomials $\Theta_1(\gamma)$ and $\Theta_2(\gamma)$ can be obtained by solving a system of linear equations as we shall see in Section VII. A rather simpler local fit is given by the function

$$\widehat{\Psi}(\gamma) = \frac{d_1}{2}\log(1 + d_2\gamma^2),$$

for $\gamma$ in a given desired range of operation, where $d_1$ and $d_2$ are to be chosen based on the desired SNR range. Clearly, $d_1 = 1$ and $d_2 = \min\left\{\frac{e\bar{\gamma}^2}{2\pi\gamma^2}, \frac{1}{2\pi e}\right\}$ at high SNR. At low SNR, $d_1$ and $d_2$ should satisfy $d_1 d_2 = \min\left\{\frac{\bar{\gamma}}{\gamma}\left(1 - \frac{\bar{\gamma}}{\gamma}\right), \frac{1}{4}\right\}$. For moderate SNR, $d_1$ and $d_2$ can be chosen for a range $\gamma \in [\gamma_1, \gamma_2]$ dB using a simple formula, and the achievable rates of $\mathcal{R}_F$ at three PSNR values, $\gamma_1$, $\gamma_2$, and $\gamma_0 \in [\gamma_1, \gamma_2]$. This function provides a very good local fit for the SNR range of interest, and can be used to study channels with weak turbulence where the SNR does not vary widely.

Section VIII compares the high-SNR capacities of a HD system and an IM-DD system. Table I summarizes the result of this comparison, and Fig. 4 shows an example.

The next sections prove the main results presented in this section.

## IV. The IM-DD Channel with a Peak Constraint

Upper bounds and lower bounds for this case have been derived in [9]. Here, we present upper bounds on the capacity based on sphere-packing arguments. We consider two approaches: one that uses the Steiner-Minkowski formula, and one that uses a recursive approach. Then, we compare the two approaches and comment on their differences.

The capacity of a channel with a peak constraint can be interpreted as a problem of packing spheres in a cube (Fig. 5a). In particular, since a codeword $\mathbf{X} = (X_1, X_2, \cdots, X_n)$ satisfies the constraint $0 \leq X_i \leq \mathcal{A}$ for $i = 1, \cdots, n$, then this codeword is confined to an $n$-dimensional cube with edge-length $\mathcal{A}$. We call this $n$-cube $\mathcal{W}_{\mathcal{A}}^n$.

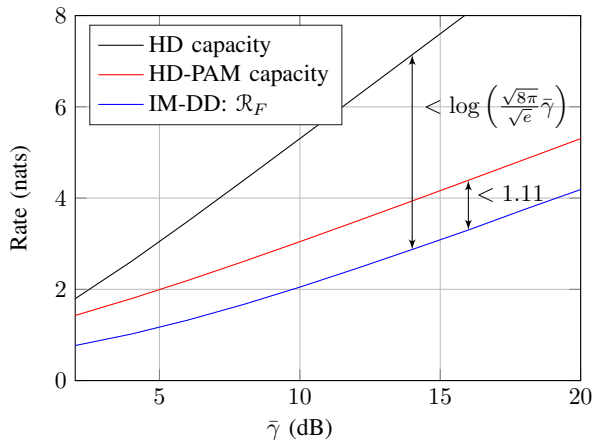


(a) $\frac{\mathcal{E}}{\mathcal{A}} = 0.1$.

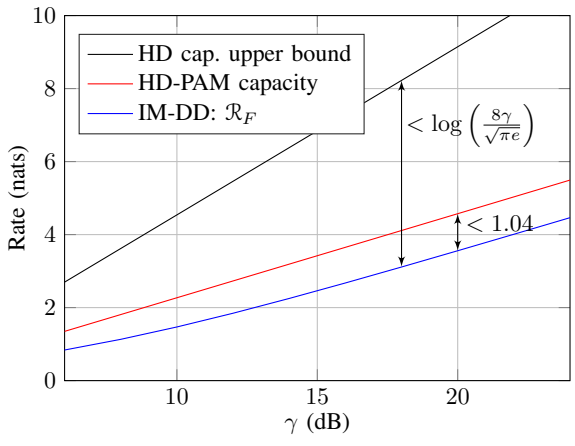


(b) $\frac{\mathcal{E}}{\mathcal{A}} = \frac{1}{2}$.

Fig. 4: High SNR behavior of the capacity of IM-DD and HD systems for $\alpha = \frac{1}{2}$. Here $\bar{\gamma} = \mathcal{E}/\sigma$ and $\gamma = \mathcal{A}/\sigma$.

On the other hand, the noise random variable $Z$ satisfies $E[Z^2] = \sigma^2$. By the law of large numbers, for every $\epsilon > 0$, $\exists N \in \mathbb{N}$ such that for $n \geq N$,

$$\left| \frac{1}{n} \sum_{i=1}^{n} Z_i^2 - \mathbb{E}[Z^2] \right| < \epsilon,$$

where $Z_i$ is the $i$-th component of the received noise sequence $\mathbf{Z}$. Therefore, $\mathbf{Z}$ has a magnitude (Euclidean norm) which approaches

$$\lambda \triangleq \sqrt{n\sigma^2}$$

for large $n$. This confines the noise 'almost certainly be to some point near the surface [25]' of an $n$-dimensional ball of radius $\lambda$, which we denote $\mathcal{B}_\lambda^n$.

Thus, the noise-perturbed signal $\mathbf{Y} = \mathbf{X} + \mathbf{Z}$ lies almost surely near the surface of a ball $\mathcal{B}_\lambda^n$ about $\mathbf{X}$. This is denoted 'decoding sphere' in [23]. An upper bound for the IM-DD channel capacity can be obtained by computing the maximum number $M_n$ of non-overlapping decoding spheres that can be packed centered in $\mathcal{W}_\mathcal{A}^n$, as $n \to \infty$ (as in [11]).[1] Here, we use the sub-script $\mathcal{A}$ to indicate that this is the capacity of the channel with only a peak intensity constraint $\mathcal{A}$.

### A. Steiner-Minkowski Formula

An upper bound on $M_n$ can be found using an idea similar to the sphere-packing argument in [23]. The main difference is that in our case we have a packing problem in a cube instead of a sphere.

[1]Appendix B explains geometrically why the capacity of a Gaussian channel can be bounded by using sphere-packing arguments.

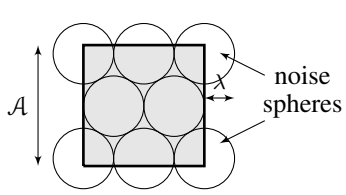


(a) Sphere-packing in a cube.

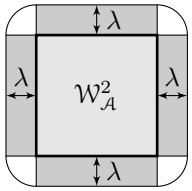


(b) The $\lambda$-neighborhood of the square is the sum of a square, a disk, and four rectangles.

Fig. 5: Packing spheres of radius $\lambda$ so that their center lie inside a cube of side-length $\mathcal{A}$. The convex envelope at a distance $\lambda$ of the cube is the $\lambda$-neighborhood of the cube.

The noise balls extend the cube by a distance of $\lambda$ in all directions. This extension is the so-called $\lambda$-neighborhood of $\mathcal{W}_{\mathcal{A}}^n$,[2] which we denote by $\mathcal{W}_{\mathcal{A}}^n(\lambda)$. By dividing the volume of $\mathcal{W}_{\mathcal{A}}^n(\lambda)$ by the volume of $\mathcal{B}_{\lambda}^n$, we get an upper bound on $M_n$. This leads to an upper bound on $\mathcal{C}_{\mathcal{A}}$ as follows:

$$\mathcal{C}_{\mathcal{A}} \leq \lim_{n\to\infty} \frac{1}{n} \log\left(\frac{V(\mathcal{W}_{\mathcal{A}}^n(\lambda))}{V(\mathcal{B}_{\lambda}^n)}\right).$$

Finding $V(\mathcal{W}_{\mathcal{A}}^n(\lambda))$ is not as straightforward as the case of a sphere. However, according to the Steiner-Minkowski theorem for polytopes [17, Proposition 12.3.6], this volume can be written as a polynomial of degree $n$ in $\lambda$. This theorem is stated as follows.

*Theorem 5 (Steiner-Minkowski [17]):* To every $n$-dimensional convex set $\mathcal{T}$, we can associate scalars $L_i(\mathcal{T})$, $i = 0, 1, \cdots, n$, such that the volume of the $\lambda$-neighborhood $\mathcal{T}'(\lambda)$ of $\mathcal{T}$, $\lambda > 0$, is given by $V(\mathcal{T}(\lambda)) = \sum_{i=0}^{n} L_i(\mathcal{T})\lambda^i$, where $L_i(\mathcal{T})$ are continuous functions.

Thus, for evaluating $V(\mathcal{W}_{\mathcal{A}}^n(\lambda))$, it remains to determine the coefficients of the Steiner-Minkowski formula. These coefficients were given in [18] for any convex body as follows.

*Theorem 6 ( [18]):* For any convex body $\mathcal{T}$ of $n$ dimensions, the coefficients of the Steiner-Minkowski formula can be written as $L_i(\mathcal{T}) = \sum_{\mathcal{T}^{n-i}\in\partial\mathcal{T}} V(\mathcal{T}^{n-i})V(\mathcal{B}_1^i)\theta_{\mathcal{T}^{n-i},\mathcal{T}}$, where $\mathcal{T}^{n-i}$ is a generic $n-i$ dimensional face of $\partial\mathcal{T}$ the boundary of $\mathcal{T}$, and $\theta_{\mathcal{T}^{n-i},\mathcal{T}}$ is the normalized dihedral external angle of $\mathcal{T}^{n-i}$ in $\mathcal{T}$.

**Example:** An example illustrating this theorem is shown in Fig. 5b. This figure shows $\mathcal{W}_{\mathcal{A}}^2(\lambda)$, the $\lambda$-neighborhood of $\mathcal{W}_{\mathcal{A}}^2$. Note that the extension of $\mathcal{W}_{\mathcal{A}}^2$ by $\lambda$ extends each vertex to a quarter of a 2-dimensional disk of radius $\lambda$, and each edge to a half of a 2-dimensional cylinder (rectangle) of length $\mathcal{A}$ and radius $\lambda$. Thus we can write

$$\begin{aligned} V(\mathcal{W}_{\mathcal{A}}^2(\lambda)) &= \mathcal{A}^2 + 4(2^{-1})\mathcal{A}^1(2\lambda) + 4(2^{-2})\mathcal{A}^0(\pi\lambda^2) \\ &= \sum_{i=0}^{n} 2^i \binom{n}{n-i} 2^{-i}\mathcal{A}^{n-i}V(\mathcal{B}_{\lambda}^i), \end{aligned}$$

with $n = 2$. In this expression, $2^i\binom{n}{n-i}$ is the number of $n-i$ dimensional faces of $\mathcal{W}_{\mathcal{A}}^n$ [17], $2^{-i}$ is the normalized dihedral external angle of the $n-i$ dimensional face in $\mathcal{W}_{\mathcal{A}}^n$ (see definition of this angle in [18]), and $\mathcal{A}^i V(\mathcal{B}_{\lambda}^i)$

[2]or the Minkowski sum of the cube and the ball

is the volume of the cylinder formed by the orthogonal product of the $n-i$ dimensional face and $\mathcal{B}_\lambda^i$. Note that the $n-i$ dimensional faces of $\mathcal{W}_\mathcal{A}^n$ are $\mathcal{W}_\mathcal{A}^{n-i}$ [17].

By extending this argument to higher dimensions, we obtain $L_i(\mathcal{W}_\mathcal{A}^n)\lambda^i = \binom{n}{n-i}\mathcal{A}^{n-i}V(\mathcal{B}_\lambda^i)$, as a special case of Theorem 6 for the cube. Now, we replace $V(\mathcal{B}_\lambda^i)$ by $\frac{(\sqrt{\pi}\lambda)^i}{\Gamma\left(1+\frac{i}{2}\right)}$ ($\Gamma(\cdot)$ is the Gamma function) and $\lambda$ by $\sqrt{n\sigma^2}$, we substitute $L_i(\mathcal{W}_\mathcal{A}^n)$ in the expression of $V(\mathcal{W}_\mathcal{A}^n(\lambda))$ according to Theorem 5, and divide by $V(\mathcal{B}_\lambda^n)$ to obtain

$$M_n \leq \sum_{i=0}^{n} N_i, \tag{6}$$

where $N_i = \binom{n}{n-i}\left(\frac{\mathcal{A}}{\sqrt{\pi n\sigma^2}}\right)^{n-i}\frac{\Gamma\left(1+\frac{n}{2}\right)}{\Gamma\left(1+\frac{i}{2}\right)}$.

Thus, we have the capacity upper bound $\mathcal{C}_\mathcal{A} \leq \lim_{n\to\infty}\frac{1}{n}\log\left(\sum_{i=0}^{n} N_i\right)$ from (6). The remaining steps are similar to [11] (given in Appendix C for completeness), and lead to

$$\lim_{n\to\infty}\frac{1}{n}\log\left(\sum_{i=0}^{n} N_i\right) \leq \sup_{\alpha\in[0,1]} B_1(\alpha), \tag{7}$$

where

$$B_1(\alpha) = \alpha\log\left(\frac{\gamma}{\sqrt{2\pi e}}\right) - \log\left(\alpha^\alpha(1-\alpha)^{\frac{3(1-\alpha)}{2}}\right),$$

which leads to the upper bound $\overline{\mathcal{C}}_{\mathcal{A},1}$ given in Theorem 1.

Note that apart from defining the $\lambda$-neighborhood of the cube $\mathcal{W}_\mathcal{A}^n$ based on the geometry of the ball, the rest of the derivation of the bound $\overline{\mathcal{C}}_{\mathcal{A},1}$ is geometry independent. In fact, the upper bound on $M_n$ in (6) can be interpreted as the number of containers of liquid of volume $V(\mathcal{B}_\lambda^n)$ that can be poured inside $V(\mathcal{W}_\mathcal{A}^n(\lambda))$. From this point of view, a different approach with better exploitation of the geometry of the ball should have an advantage over this one, at least in some cases. Next, we present a bound based on a recursive sphere-packing approach.

### *B. A Recursive Approach*

Recall that an upper bound on the channel capacity can be obtained by computing the maximum number $M_n$ of non-overlapping balls that can be packed centered in $\mathcal{W}_\mathcal{A}^n$, as $n\to\infty$ [11], [23], [25]. Consider an arbitrary constellation of non-overlapping balls $\mathcal{B}_\lambda^n$ with their centers in $\mathcal{W}_\mathcal{A}^n$. We upper bound the number of balls $M_n$ by upper bounding the volume of balls and then dividing by $V(\mathcal{B}_\lambda^n)$. The total volume of such balls can be written as

$$v_{\text{tot}} = v_{\text{in}}(\mathcal{W}_\mathcal{A}^n) + v_{\text{out}}(\mathcal{W}_\mathcal{A}^n), \tag{8}$$

where $v_{\text{in}}(\mathcal{W}_\mathcal{A}^n)$ is the volume of balls and portions of balls inside $\mathcal{W}_\mathcal{A}^n$, and $v_{\text{out}}(\mathcal{W}_\mathcal{A}^n)$ is the volume of portions of balls outside $\mathcal{W}_\mathcal{A}^n$. Clearly, $v_{\text{in}}(\mathcal{W}_\mathcal{A}^n) \leq V(\mathcal{W}_\mathcal{A}^n)$ (shaded area in the 2-dimensional illustration in Fig. 6a). Now we upper bound $v_{\text{out}}(\mathcal{W}_\mathcal{A}^n)$ (un-shaded areas in Fig. 6a).

Consider one $(n-1)$-dimensional face $\mathcal{W}_\mathcal{A}^{n-1}$ of $\mathcal{W}_\mathcal{A}^n$. Our goal is to transform the problem of bounding $v_{\text{out}}(\mathcal{W}_\mathcal{A}^n)$ to a problem of packing $(n-1)$-balls in $\mathcal{W}_\mathcal{A}^{n-1}$. To this end, we distribute the portions of balls outside $\mathcal{W}_\mathcal{A}^n$ between the faces, by associating each portion to the face with which it has the largest intersection (see Fig. 6b). Next, we upper bound the volumes of these portions by twice the volumes of the spherical-caps[3] on the outer side of the

[3]A spherical-cap is defined as the portion of an $n$-sphere cut by an $(n-1)$-plane.

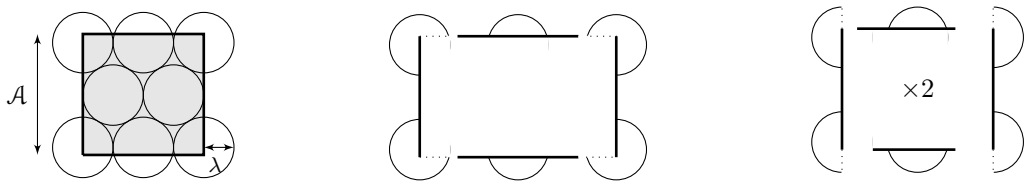


(a) Balls $\mathcal{B}_\lambda^2$ packed in $\mathcal{W}_\mathcal{A}^2$.

(b) Portions of balls outside $\mathcal{W}_\mathcal{A}^2$ distributed between its faces.

(c) Upper bound for the portions in Fig. 6b.

Fig. 6: A 2-dimensional illustration of the recursive approach.

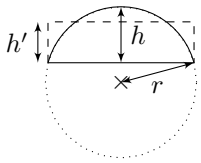


Fig. 7: A spherical-cap in 2-dimensions of radius $r$ and height $h$, and the corresponding equivalent cylinder (rectangle in the 2-dimensional case) of height $h'$.

face (see Fig. 6c), where we multiply by 2 to account for the portions overflowing to the other side of this face. Thus, we have

$$v_{\text{out}}(\mathcal{W}_\mathcal{A}^n) \leq 2 \sum_{\mathcal{W}_\mathcal{A}^{n-1} \subset \partial \mathcal{W}_\mathcal{A}^n} V(\text{spherical-caps on } \mathcal{W}_\mathcal{A}^{n-1}), \tag{9}$$

where $\partial \mathcal{W}_\mathcal{A}^n$ is the boundary of $\mathcal{W}_\mathcal{A}^n$. Hence,

$$v_{\text{tot}} \leq V(\mathcal{W}_\mathcal{A}^n) + 2 \sum_{\mathcal{W}_\mathcal{A}^{n-1} \subset \partial \mathcal{W}_\mathcal{A}^n} V(\text{spherical-caps on } \mathcal{W}_\mathcal{A}^{n-1}). \tag{10}$$

Next, we upper bound $V(\text{spherical-caps on } \mathcal{W}_\mathcal{A}^{n-1})$. Denote the volume of an $n$-dimensional spherical-cap of height $h$ and radius $\lambda$ (see Fig. 11b) by $V(\mathcal{P}_{\lambda,h}^n)$. We transform each spherical-cap to an equivalent cylinder which has the same base as the spherical-cap, but different height $h'$, so that both have the same volume. The height $h'$ of this cylinder is $h' = \frac{V(\mathcal{P}_{\lambda,h}^n)}{V(\mathcal{B}_{\lambda'}^{n-1})}$, where $\lambda' = \sqrt{2h\lambda - h^2}$, since the base of the spherical-cap is $\mathcal{B}_{\lambda'}^{n-1}$. In Appendix D, we show that $h' \leq \hat{h}_n$ where $\hat{h}_n$ is the height of the equivalent cylinder corresponding to a spherical cap $\mathcal{P}_{\lambda,\lambda}^n$. Thus

$$h' \leq \hat{h}_n = \frac{V(\mathcal{B}_\lambda^n)}{2V(\mathcal{B}_\lambda^{n-1})}. \tag{11}$$

Therefore, we can write $V(\mathcal{P}_{\lambda,h}^n) \leq \hat{h}_n V(\mathcal{B}_{\lambda'}^{n-1})$.

Now we get back to bounding $V(\text{spherical-caps on } \mathcal{W}_\mathcal{A}^{n-1})$. Denote the heights of spherical-caps on $\mathcal{W}_\mathcal{A}^{n-1}$ by

$h_1, \cdots, h_a$ where $a \in \mathbb{N}$ is the number of such caps. Then, we can write

$$V(\text{spherical-caps on } \mathcal{W}_{\mathcal{A}}^{n-1}) = \sum_{i=1}^{a} V(\mathcal{P}_{\lambda,h_i}^{n}) \tag{12}$$

$$\leq \hat{h}_n \sum_{i=1}^{a} V(\mathcal{B}_{\lambda_i'}^{n-1}), \tag{13}$$

where $\lambda_i' = \sqrt{2h_i\lambda - h_i^2}$. This step upper bounds the $a$ spherical-caps by $a$ cylinders with larger volume and same intersection with $\mathcal{W}_{\mathcal{A}}^{n-1}$. At this point, we have a constellation of $a$ balls of dimension $n-1$, whose radii are $\lambda_i'$, $i = 1, \cdots, a$, and which are centered in $\mathcal{W}_{\mathcal{A}}^{n-1}$. The total volume of those balls can be upper bounded by repeating the same steps above. Thus,

$$V(\text{spherical-caps on } \mathcal{W}_{\mathcal{A}}^{n-1}) \leq \hat{h}_n \left[ V(\mathcal{W}_{\mathcal{A}}^{n-1}) + v_{\text{out}}(\mathcal{W}_{\mathcal{A}}^{n-1}) \right]. \tag{14}$$

Here, $v_{\text{out}}(\mathcal{W}_{\mathcal{A}}^{n-1})$ is the volume of portions of the $a$ balls of $n-1$ dimensions outside $\mathcal{W}_{\mathcal{A}}^{n-1}$. We plug this in (10) to obtain

$$v_{\text{tot}} \leq V(\mathcal{W}_{\mathcal{A}}^{n}) + 2\hat{h}_n \sum_{\mathcal{W}_{\mathcal{A}}^{n-1} \subset \partial \mathcal{W}_{\mathcal{A}}^{n}} \left[ V(\mathcal{W}_{\mathcal{A}}^{n-1}) + v_{\text{out}}(\mathcal{W}_{\mathcal{A}}^{n-1}) \right] \tag{15}$$

$$= \sum_{i=0}^{1} 2^i K_{n-i} V(\mathcal{W}_{\mathcal{A}}^{n-i}) \prod_{j=0}^{i} \hat{h}_{n+1-j} + 2\hat{h}_n \sum_{\mathcal{W}_{\mathcal{A}}^{n-1} \subset \partial \mathcal{W}_{\mathcal{A}}^{n}} v_{\text{out}}(\mathcal{W}_{\mathcal{A}}^{n-1}), \tag{16}$$

where $K_{n-1}$ is the number of $(n-1)$-faces in $\mathcal{W}_{\mathcal{A}}^{n}$, and where we formally define $\hat{h}_{n+1} = 1$.

*Remark 3:* While the Steiner-Minkowski approach calculates the volume of the parallel extension of $\mathcal{W}_{\mathcal{A}}^{n-1}$ of thickness $\lambda$, here we have thickness $2\hat{h}_n$ instead, which is smaller than $\lambda$ for $n$ large enough.

Similar to (9), we can show that

$$\sum_{\mathcal{W}_{\mathcal{A}}^{n-1} \subset \partial \mathcal{W}_{\mathcal{A}}^{n}} v_{\text{out}}(\mathcal{W}_{\mathcal{A}}^{n-1}) \leq 2 \sum_{\mathcal{W}_{\mathcal{A}}^{n-2} \subset \partial \mathcal{W}_{\mathcal{A}}^{n}} V(\text{spherical-caps on } \mathcal{W}_{\mathcal{A}}^{n-2}). \tag{17}$$

This can be shown by joining the $(n-1)$-faces of $\mathcal{W}_{\mathcal{A}}^{n}$ back together, and redistributing the portions of the $(n-1)$-balls over the $(n-2)$-faces of $\mathcal{W}_{\mathcal{A}}^{n}$ in a fashion similar to Fig. 6b. Using (14) again leads to[4]

$$v_{\text{tot}} \leq \sum_{i=0}^{2} 2^i K_{n-i} V(\mathcal{W}_{\mathcal{A}}^{n-i}) \prod_{j=0}^{i} \hat{h}_{n+1-j} + 4\hat{h}_n \hat{h}_{n-1} \sum_{\mathcal{W}_{\mathcal{A}}^{n-2} \subset \partial \mathcal{W}_{\mathcal{A}}^{n}} v_{\text{out}}(\mathcal{W}_{\mathcal{A}}^{n-2}) \tag{18}$$

$$= \sum_{i=0}^{\ell} 2^i K_{n-i} V(\mathcal{W}_{\mathcal{A}}^{n-i}) \prod_{j=0}^{i} \hat{h}_{n+1-j} + 2^\ell \prod_{j=0}^{\ell} \hat{h}_{n+1-j} \sum_{\mathcal{W}_{\mathcal{A}}^{n-\ell} \subset \partial \mathcal{W}_{\mathcal{A}}^{n}} v_{\text{out}}(\mathcal{W}_{\mathcal{A}}^{n-\ell}) \tag{19}$$

with $\ell = 2$. By proceeding similarly, we can write for $\ell = n-1$

$$v_{\text{tot}} \leq \sum_{i=0}^{n-1} 2^i K_{n-i} V(\mathcal{W}_{\mathcal{A}}^{n-i}) \prod_{j=0}^{i} \hat{h}_{n+1-j} + 2^{n-1} \prod_{j=0}^{n-1} \hat{h}_{n+1-j} \sum_{\mathcal{W}_{\mathcal{A}}^{1} \subset \partial \mathcal{W}_{\mathcal{A}}^{n}} v_{\text{out}}(\mathcal{W}_{\mathcal{A}}^{1}). \tag{20}$$

Similar to (17), we have

$$\sum_{\mathcal{W}_{\mathcal{A}}^{1} \subset \partial \mathcal{W}_{\mathcal{A}}^{n}} v_{\text{out}}(\mathcal{W}_{\mathcal{A}}^{n-1}) \leq 2 \sum_{\mathcal{W}_{\mathcal{A}}^{0} \subset \partial \mathcal{W}_{\mathcal{A}}^{n}} V(\text{spherical-caps on } \mathcal{W}_{\mathcal{A}}^{0}). \tag{21}$$

[4]Note that $\hat{h}_n$ is increasing in $\lambda$. Thus, the equivalent height of a spherical-cap with radius $\lambda' < \lambda$ is also less than $\hat{h}_n$.

Since $V(\text{spherical-caps on } \mathcal{W}_{\mathcal{A}}^0)$ is upper bounded by $\hat{h}_1$, we obtain

$$v_{\text{tot}} \leq \sum_{i=0}^{n} 2^i K_{n-i} V(\mathcal{W}_{\mathcal{A}}^{n-i}) \prod_{j=0}^{i} \hat{h}_{n+1-j}. \tag{22}$$

By noting that $2^i \prod_{j=0}^{i} \hat{h}_{n+1-j} = \frac{V(\mathcal{B}_\lambda^n)}{V(\mathcal{B}_\lambda^{n-i})}$, and using $K_{n-i} = 2^i \binom{n}{n-i}$, we obtain

$$v_{\text{tot}} \leq \sum_{i=0}^{n} 2^i \binom{n}{n-i} V(\mathcal{W}_{\mathcal{A}}^{n-i}) \frac{V(\mathcal{B}_\lambda^n)}{V(\mathcal{B}_\lambda^{n-i})}. \tag{23}$$

Now, we divide by $V(\mathcal{B}_\lambda^n)$, and to obtain the following upper bound on $M_n$,

$$M_n \leq \sum_{i=0}^{n} 2^i \binom{n}{n-i} \frac{V(\mathcal{W}_{\mathcal{A}}^{n-i})}{V(\mathcal{B}_\lambda^{n-i})}. \tag{24}$$

By replacing $V(\mathcal{W}_{\mathcal{A}}^{n-i})$ by $\mathcal{A}^{n-i}$, $V(\mathcal{B}_\lambda^{n-i})$ by $\frac{(\sqrt{\pi}\lambda)^n}{\Gamma\left(1+\frac{n}{2}\right)}$, $\lambda$ by $\sqrt{n\sigma^2}$, and proceeding similar to [11] (see Appendix C), we obtain the upper bound $\mathcal{C}_{\mathcal{A}} \leq \overline{\mathcal{C}}_{\mathcal{A},2} = \sup_{\alpha\in[0,1]} B_2(\alpha)$, where

$$B_2(\alpha) = \alpha \log\left(\frac{\gamma}{\sqrt{2\pi e}}\right) - \log\left(\alpha^{\frac{\alpha}{2}} (1-\alpha)^{1-\alpha} 2^{\alpha-1}\right)$$

as given in Theorem 1.

### C. Comparison

Note that both $\overline{\mathcal{C}}_{\mathcal{A},1}$ and $\overline{\mathcal{C}}_{\mathcal{A},2}$ are tight at high PSNR $\gamma$, since both converge to the lower bound [9, Theorem 5] given by $\mathcal{C}_{\mathcal{A}} \geq \frac{1}{2}\log\left(1+\frac{\gamma^2}{2\pi e}\right)$. This is also true for a channel with both a peak and an average constraint, with $\mathcal{A} \leq 2\mathcal{E}$. Note also that $\overline{\mathcal{C}}_{\mathcal{A},2}$ becomes tighter than $\overline{\mathcal{C}}_{\mathcal{A},1}$ when the optimum $\alpha$ is close to 1. This is the case at moderate/high PSNR where the first term of $B_1(\alpha)$ and $B_2(\alpha)$ dominates the bound. This behavior can be justified by remark 3, which is in turn due to exploiting the geometry of the sphere in the recursive approach. At low PSNR, $\overline{\mathcal{C}}_{\mathcal{A},1}$ is tighter than $\overline{\mathcal{C}}_{\mathcal{A},2}$. The reason is that in the recursive approach, we place a ball on each vertex of the cube (see (21)). Thus, the upper bound on $M_n$ is larger than $2^n$ at any PSNR. At low PSNR, this term dominates, and $\overline{\mathcal{C}}_{\mathcal{A},2}$ converges to $\log(2)$ (not to zero as for $\overline{\mathcal{C}}_{\mathcal{A},1}$). The next section applies the recursive approach to bound the capacity of the channel with only an average constraint, and proves Theorem 2.

## V. Average Constraint

Now we consider an IM-DD channel with only an average intensity constraint. The capacity of this case can be interpreted as a problem of packing spheres in a simplex. A sphere-packing upper bound was derived in [11] using the Steiner-Minkowski formula. Next, we derive an upper bound using the recursive approach as in Section IV-B, and show that this bound is tighter than the one given in [11] for all ASNR.

### A. A Recursive Approach

For a channel with an average constraint only, we have $\mathcal{A} = \infty$. Thus, according to Lemma 1, the optimal distribution satisfies $\mathbb{E}[X] = \mathcal{E}$. On the other hand, by the law of large numbers, for every $\epsilon > 0$, $\exists N \in \mathbb{N}$ such that

$$\left|\frac{1}{n}\sum_{i=1}^{n} X_i - \mathbb{E}[X]\right| \leq \epsilon,$$

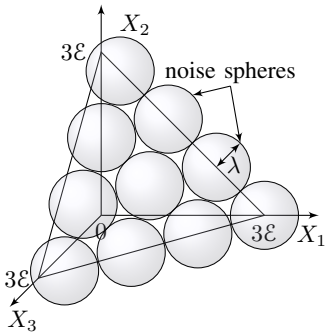


(a) Balls $\mathcal{B}_\lambda^3$ packed centered on the 2-simplex $\mathcal{S}_\mathcal{E}^2$ defined by $\sum_{i=1}^3 X_i = 3\mathcal{E}$.

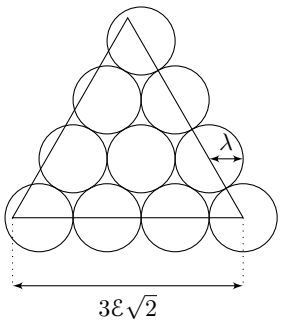


(b) Balls $\mathcal{B}_\lambda^2$ packed on a regular 2-simplex $\mathcal{S}_\mathcal{E}^2$ with side-length $3\mathcal{E}\sqrt{2}$.

Fig. 8

for $n \geq N$. Thus, since a codeword $\mathbf{X} = (X_1, X_2, \cdots, X_n)$ satisfies $\mathbb{E}[X] = \mathcal{E}$, then for large $n$, our codewords satisfy $X_i \geq 0$, and $\sum_{i=1}^n X_i = n\mathcal{E}$ almost certainly. This confines the codewords to a regular $(n-1)$-simplex $\mathcal{S}_\mathcal{E}^{n-1} = \left\{\mathbf{X} \in \mathbb{R}_+^n \,|\sum_{i=1}^n X_i = n\mathcal{E}\right\}$ with side-length $n\mathcal{E}\sqrt{2}$ (Fig. 8a shows an example with $n = 3$). Here, we need to upper bound the number $M_n$ of balls $\mathcal{B}_\lambda^n$ that can be packed with their centers within $\mathcal{S}_\mathcal{E}^{n-1}$. Note that the intersection of an $n$-ball with the $(n-1)$-dimensional hyperplane supporting $\mathcal{S}_\mathcal{E}^{n-1}$ is $\mathcal{B}_\lambda^{n-1}$. Thus, the problem is equivalent to bounding the number of $\mathcal{B}_\lambda^{n-1}$ that can be packed centered in $\mathcal{S}_\mathcal{E}^{n-1}$ (see Fig. 8b.

We apply our recursive approach to bound $M_n$. Similar to Section IV-B, we bound $M_n$ by bounding the volume of balls that can be packed centered in $\mathcal{S}_\mathcal{E}^{n-1}$ and then divide by $V(\mathcal{B}_\lambda^{n-1})$. The same steps as (8)-(23) can now be applied to this case. The volume of balls and portions of balls inside $\mathcal{S}_\mathcal{E}^{n-1}$ can be upper bounded by $V(\mathcal{S}_\mathcal{E}^{n-1})$. The portions that extend outwards of $\mathcal{S}_\mathcal{E}^{n-1}$ are distributed among the $(n-2)$-dimensional faces of $\mathcal{S}_\mathcal{E}^{n-1}$, and bounded by twice the volumes of spherical-caps on the outer side of each face. The spherical-caps are bounded by cylinders, which leads to a problem of packing $(n-2)$-dimensional balls (of different radii) on the $(n-2)$-dimensional faces of $\mathcal{S}_\mathcal{E}^{n-1}$. This procedure is repeated for all $(n-1-i)$-dimensional faces, $i = 0, \cdots, n-1$. Note that the number of $(n-i)$-dimensional faces, $i = 0, \cdots, n-1$, in $\mathcal{S}_\mathcal{E}^{n-1}$ is $\binom{n}{n-i}$, and that each such face is in fact an $(n-i)$-simplex [17]. This leads to the following upper bound on the total volume of balls

$$v_{\text{tot}} \leq \sum_{i=0}^{n-1} \binom{n}{n-i} V(\mathcal{S}_\mathcal{E}^{n-i}) \frac{V(\mathcal{B}_\lambda^n)}{V(\mathcal{B}_\lambda^{n-i})}. \tag{25}$$

By dividing by $V(\mathcal{B}_\lambda^n)$, we obtain the following upper bound on $M_n$

$$M_n \leq \sum_{i=0}^{n-1} \binom{n}{n-i} \frac{V(\mathcal{S}_\mathcal{E}^{n-i})}{V(\mathcal{B}_\lambda^{n-i})}. \tag{26}$$

Using $V(\mathcal{S}_\mathcal{E}^{n-i}) = \frac{(n\mathcal{E})^{n-i}}{(n-i)!}\sqrt{n-i+1}$ [26], $V(\mathcal{B}_\lambda^{n-i}) = \frac{(\sqrt{\pi}\lambda)^n}{\Gamma\left(1+\frac{n}{2}\right)}$, $\lambda = \sqrt{n\sigma^2}$, and proceeding similar to Appendix C, we obtain the upper bound $\mathcal{C}_\mathcal{E} \leq \overline{\mathcal{C}}_\mathcal{E} = \sup_{\alpha\in[0,1]} B_3(\alpha)$, where $B_3(\alpha) = \alpha \log\left(\frac{\sqrt{e}\bar{\gamma}}{\sqrt{2\pi}}\right) - \log\left((1-\alpha)^{1-\alpha}\alpha^{\frac{3\alpha}{2}}\right)$ as given in Theorem 2.

*Remark 4:* If we use $\mathbb{E}[X] \leq \mathcal{E}$ instead of $\mathbb{E}[X] = \mathcal{E}$, we get the right $n$-simplex $\hat{\mathcal{S}}_{\mathcal{E}}^n = \{\mathbf{X} \in \mathbb{R}_+^n | \sum_{i=1}^n X_i \leq n\mathcal{E}\}$. A sphere-packing bound for this case was derived in [11] using the Steiner-Minkowski formula. Our approach can also be applied on this right $n$-simplex. Alternatively, we can outer bound this right $n$-simplex by replacing the vertex at the origin with a vertex at $-(d, d, \cdots, d)$ where $d = (\sqrt{n+1} - 1)\mathcal{E}$ to obtain a regular $n$-simplex $\mathcal{S}_{\mathcal{E}}^n$, and then apply our recursive approach to this simplex. This yields the same bound as (26).

*Remark 5:* Note that this approach avoids using the external normalized dihedral angle, which is difficult to compute in a simplex. This is contrary to the approach using the Steiner-Minkowski formula (see equation (6) in [11] e.g.).

### *B. Comparison*

As discussed in Section III, this bound is tighter than the one derived in [11] using the Steiner-Minkowski formula for any ASNR. Again, the main reason is that this recursive approach is more dependent on the geometry of the ball than the approach used in [11]. The bound $\overline{\mathcal{C}}_{\mathcal{E}}$ characterizes the high ASNR capacity for a channel with *only* an average constraint. Namely, at high ASNR, $B_3(\alpha)$ converges to $\alpha \log\left(\frac{\sqrt{e\bar{\gamma}}}{\sqrt{2\pi}}\right)$, and therefore, $\overline{\mathcal{C}}_{\mathcal{E}}$ approaches $\frac{1}{2}\log\left(\frac{e\bar{\gamma}^2}{2\pi}\right)$ where it meets the lower bound [9, Theorem 7] given by $\mathcal{C}_{\mathcal{E}} \geq \frac{1}{2}\log\left(1 + \frac{e\bar{\gamma}^2}{2\pi}\right)$.

Recall that using the recursive approach, the bound on $M_n$ is dominated by the number of vertexes at low SNR. Since the number of vertexes of the simplex scales linearly with its dimensions, our bound $\overline{\mathcal{C}}_{\mathcal{E}}$ approaches zero at low ASNR. This is in contrast with $\overline{\mathcal{C}}_{\mathcal{A},2}$ which does not approach zero since the number of vertexes of a cube scales exponentially with its dimensions. Next, we consider an IM-DD channel with both average and peak constraints.

## VI. Average and Peak Constraints

Upper bounds on the capacity of the channel with both average and peak constraints were given in [9]. Next, we provide an alternative derivation of one of the bounds in [9], based on the variance maximizing distribution in $\mathcal{F}$.

### *A. Alternative Derivation of [9, (11) & (19)]*

The capacity of the channel is given by $\mathcal{C} = \max_{f(x)\in\mathcal{F}} I(X;Y)$ [23]. The capacity maximizing input distribution is not known for this channel. However, we know that if $X$ can be unbounded, and it satisfies only a variance constraint $\text{Var}(X) \leq P$, then the maximizing input distribution is $g_{0,\sqrt{P}}(x)$. By assuming that the input of our IM-DD channel satisfies $\text{Var}(X) \leq P$ for some $P > 0$, and by ignoring the constraint $X \in [0, \mathcal{A}]$, we can write the upper bound $\mathcal{C} \leq \frac{1}{2}\log\left(1 + \frac{P}{\sigma^2}\right)$.

The problem boils down to finding the maximum allowable variance for $f(x) \in \mathcal{F}$. The distribution $f(x) \in \mathcal{F}$ with mean $\mathbb{E}[X] = \mu$ that has maximum variance is the binary distribution $f_\mu(x)$ where $f_\mu(\mathcal{A}) = \frac{\mu}{\mathcal{A}}$ and $f_\mu(0) = 1 - \frac{\mu}{\mathcal{A}}$.

In particular, for any distribution $f(x)$ with support $\mathcal{X} \subseteq [0, \mathcal{A}]$ and mean $\mu$, the variance is upper bounded by

$$\begin{aligned} \text{Var}(X) &= \int_{x\in\mathcal{X}} (x-\mu)^2 f(x)dx && (27)\\ &\leq \int_{x\in\mathcal{X}} \left[\frac{x}{\mathcal{A}}(\mathcal{A}-\mu)^2 + \left(1-\frac{x}{\mathcal{A}}\right)\mu^2\right] f(x)dx && (28)\\ &= \mu(\mathcal{A}-\mu), && (29)\end{aligned}$$

with equality of if $f(x) = f_\mu(x)$. Now since $\mu \leq \mathcal{E}$, then the variance of $X \sim f_\mu(x)$ is maximized if $\mu = \frac{\mathcal{A}}{2}$ when $\frac{\mathcal{E}}{\mathcal{A}} \geq \frac{1}{2}$ and $\mu = \mathcal{E}$ otherwise. This leads to the same upper bound in [9, (11) & (19)] as given in Theorem 3.

Next, we derive the rate achievable by using a truncated-Gaussian (TG) input distribution, and show that it is within a negligible gap of capacity at high SNR.

### *B. Truncated-Gaussian*

We consider a distribution of $X$ given by

$$\tilde{g}_{\mu,\nu}(x) = \eta g_{\mu,\nu}(x), \quad x \in [0, \mathcal{A}], \tag{30}$$

for some $\mu \in \mathbb{R}$ and $\nu \in \mathbb{R}_+$, where $\eta$ is given by $\eta = (G_{\mu,\nu}(\mathcal{A}) - G_{\mu,\nu}(0))^{-1}$. The mean of this distribution is

$$\tilde{\mu} = \int_0^{\mathcal{A}} x\tilde{g}_{\mu,\nu}(x)dx = \nu^2\eta(g_{\mu,\nu}(0) - g_{\mu,\nu}(\mathcal{A})) + \mu. \tag{31}$$

We choose $\mu$ and $\nu$ such that $\tilde{\mu} \leq \min\{\mathcal{E}, \frac{\mathcal{A}}{2}\}$ as stated in Theorem 4. For a given choice of $\mu$ and $\nu$, we can express the achievable rate as [23]

$$R = I(X;Y) = \int_0^{\mathcal{A}} \int_{-\infty}^{\infty} f(x,y) \log\left(\frac{f(y|x)}{f(y)}\right) dydx, \tag{32}$$

where $f(x,y) = \eta g_{\mu,\nu}(x) f(y|x)$ is the joint distribution of $(X,Y)$, $f(y|x) = g_{x,\sigma}(y)$ is the conditional distribution of $Y$ given $X$, and $f(y)$ is the marginal distribution of the channel output $Y$. To evaluate this rate, we need to find the distribution of $Y$. This can be calculated as follows:

$$f(y) = \int_0^{\mathcal{A}} f(x)f(y|x)dx = \eta g_{\mu,\sigma_y}(y)(G_{\mu',\nu'}(\mathcal{A}) - G_{\mu',\nu'}(0)), \tag{33}$$

where $\sigma_y = \sqrt{\nu^2+\sigma^2}$, $\mu' = \frac{\mu\sigma^2 + y\nu^2}{\nu^2+\sigma^2}$, and $\nu' = \frac{\nu\sigma}{\sqrt{\nu^2+\sigma^2}}$. By substituting $f(y)$ and $f(y|x)$ in (32) and evaluating (remaining details are relegated to Appendix E), we get the statement of Theorem 4 given by the achievable rate

$$\mathcal{R} = \mathcal{C}_0(\nu) - \Phi_1(\mu,\nu) - \Phi_2(\mu,\nu) - \Phi_3(\mu,\nu),$$

where $\mathcal{C}_0(\nu) = \frac{1}{2}\log\left(1+\frac{\nu^2}{\sigma^2}\right)$, $\Phi_1(\mu,\nu) = \log(\eta)$,

$$\Phi_2(\mu,\nu) = \left((\mathcal{A}-\mu)g_{\mu,\nu}(\mathcal{A}) + \mu g_{\mu,\nu}(0)\right)\frac{\eta\nu^2}{2(\nu^2+\sigma^2)},$$

and $\Phi_3(\mu,\nu) = \mathbb{E}_{X,Y}\left[\log(G_{\mu',\nu'}(\mathcal{A}) - G_{\mu',\nu'}(0))\right]$ with the expectation taken with respect to the distribution $f(x,y) = \eta g_{\mu,\nu}(x) g_{x,\sigma}(y)$.

Since $\Phi_3(\mu,\nu) < 0$, a more easily computable achievable rate can be obtained by dropping the term $\Phi_3(\mu,\nu)$ leading to

$$\mathcal{R}' = \mathcal{C}_0(\nu) - \Phi_1(\mu,\nu) - \Phi_2(\mu,\nu).$$

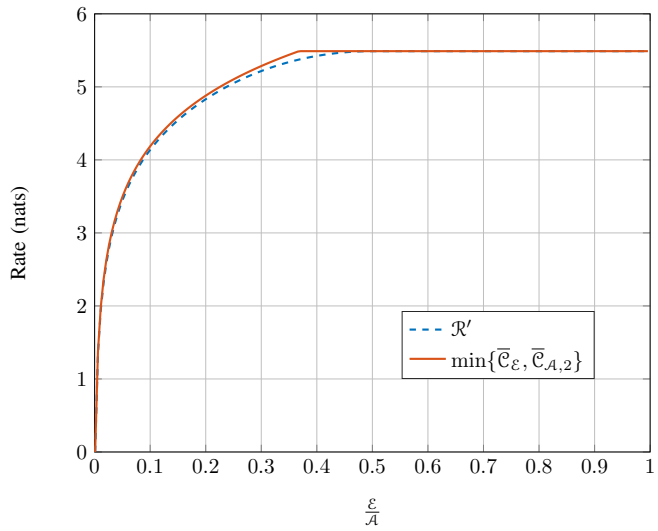


Fig. 9: Achievable rate of TG distribution and the sphere-packing upper bounds at $\mathcal{A}/\sigma = 30$dB versus the ratio $\frac{\mathcal{E}}{\mathcal{A}}$. The lower bound is obtained by fixing $\mu = 0$ and optimizing numerically with respect to $\nu$.

This achievable rate is close to capacity at high SNR (see Fig. 9). In particular, it is close to the sphere-packing bounds at high SNR. Interestingly, fixing $\mu = 0$ and optimizing with respect to $\nu$ suffices for approaching capacity at high SNR. Next, we simplify $\mathcal{R}'$ for the purpose of comparison with upper bounds at high SNR.

### *C. Simplification at High SNR*

The achievable rate $\mathcal{R}'$ can be thought of as the sum of two quantities: (i) the capacity of a Gaussian channel with Gaussian distributed input with variance $\nu^2$ ($\mathcal{C}_0(\nu)$), and (ii) residual terms which arise due to the truncation of the Gaussian distribution. With this interpretation, it is natural to check whether it is possible to make the residual terms vanish, leading to a simpler rate $\mathcal{R} \approx \mathcal{C}_0(\nu)$.

Intuitively, the rate $\mathcal{C}_0(\nu)$ is achieved if the distributions $\tilde{g}_{\mu,\nu}(x)$ and $g_{\mu,\nu}(x)$ are almost identical. Thus, we need to choose $\mu$ and $\nu$ so that $G_{\mu,\nu}(0) \approx 0$ and $G_{\mu,\nu}(\mathcal{A}) \approx 1$. Since most of the mass of the Gaussian distribution $g_{\mu,\nu}(x)$ lies between $\mu - 3\nu$ and $\mu + 3\nu$, we choose $\mu = \min\left\{\frac{\mathcal{A}}{2}, \mathcal{E}\right\} - \xi$ and $\nu = \frac{\mu}{3}$, where $\xi$ is chosen so that the average intensity $\tilde{\mu}$ (31) is equal to $\min\{\mathcal{E}, \frac{\mathcal{A}}{2}\}$. Clearly, if $\frac{\mathcal{E}}{\mathcal{A}} \geq \frac{1}{2}$, then $\xi = 0$. Otherwise, a small $\xi$ suffices to satisfy the average constraint since $g_{\mu,\nu}(x)$ and $\tilde{g}_{\mu,\nu}(x)$ are almost identical, and their means are very close.

This choice leads to $\eta \leq 1.0027$ with equality when $\mu = \mathcal{A}/2$, and thus $\Phi_1(\mu,\nu) \leq 2.7 \times 10^{-3}$. On the other hand, this choice leads to $\mu g_{\mu,\nu}(0) = \frac{3}{e^4\sqrt{2e\pi}} \geq (\mathcal{A} - \mu) g_{\mu,\nu}(\mathcal{A})$ with equality if $\mu = \mathcal{A}/2$. Thus, $\Phi_2(\mu,\nu) \leq \frac{3}{e^4\sqrt{2e\pi}} \frac{\eta\nu^2}{\nu^2+\sigma^2}$. For high SNR, $\Phi_1(\mu,\nu) + \Phi_2(\mu,\nu) < 0.016$ is negligible with respect to $\mathcal{C}_0(\nu)$. This leads to

$$\mathcal{R} \geq \mathcal{R}' > \mathcal{C}_0\left(\min\left\{\frac{\mathcal{A}}{2}, \mathcal{E}\right\}\right). \tag{34}$$

If $\frac{\mathcal{E}}{\mathcal{A}} < \frac{1}{2}$, then the achievable rate (34) becomes $\frac{1}{2}\log\left(\frac{\bar{\gamma}^2}{9}\right)$ at high SNR. This achievable rate is within $< 0.68$ nats of the upper bound $\overline{\mathcal{C}}_{\mathcal{E}}$ (Theorem 2) at high SNR. Otherwise, if $\frac{\mathcal{E}}{\mathcal{A}} \geq \frac{1}{2}$, then the achievable rate (34) is $\frac{1}{2}\log\left(\frac{\gamma^2}{36}\right)$, which is within $< 0.38$ nats of the upper bound $\overline{\mathcal{C}}_{\mathcal{A},2}$ (Theorem 1).

| $\frac{\mathcal{E}}{\mathcal{A}}$ | $\left(0, \sqrt{\frac{2}{9\pi}}\right]$ | $\left(\sqrt{\frac{2}{9\pi}}, \frac{1}{3.2}\right]$ | $\left(\frac{1}{3.2}, \frac{1}{e}\right]$ | $\left(\frac{1}{e}, \frac{1}{2}\right)$ | $\frac{1}{2}$ |
|---|---|---|---|---|---|
| $\mu$ | $0$ | $0$ | $0$ | $\frac{\mathcal{A}}{4}$ | $\frac{\mathcal{A}}{2}$ |
| $\nu$ | $\sqrt{\frac{\pi}{2}}\mathcal{E}$ | $\sqrt{\frac{\pi}{2}}\mathcal{E}$ | $\sqrt{\frac{\pi}{2}}\mathcal{E}$ | $\frac{\mathcal{A}}{3}$ | $\mathcal{A}$ |
| $\min\{\overline{\mathcal{C}}_{\mathcal{E}}, \overline{\mathcal{C}}_{\mathcal{A},2}\} - \mathcal{R}'$ | $< 0.062$ | $< 0.099$ | $< 0.163$ | $< 0.144$ | $\approx 0$ |

TABLE II: Selections of $\mu$ and $\nu$ that lead to $\mathcal{R}'$ close to capacity at high SNR.

Although the bound (34) is simple, and is within a constant of capacity at high SNR, it is not as close to capacity as one desires. Table II gives selections of $\mu$ and $\nu$ that bring $\mathcal{R}'$ closer to capacity at high SNR. The calculation of the gap $\min\{\overline{\mathcal{C}}_{\mathcal{E}}, \overline{\mathcal{C}}_{\mathcal{A},2}\} - \mathcal{R}'$ for $\frac{\mathcal{E}}{\mathcal{A}} \in \left(0, \sqrt{\frac{2}{9\pi}}\right]$ is given in Appendix F. The gap for the other cases can be obtained similarly.

By maximizing numerically with respect to $\mu$ and $\nu$, the gap to the sphere-packing bounds at high SNR can be sharpened to $< 0.1$ nats as shown in Fig. 2. Furthermore, by incorporating the upper bound $\overline{\mathcal{C}}_{L,1}$ given in [9, (12)] into the comparison, the gap $\Delta' = \min\{\overline{\mathcal{C}}_{\mathcal{E}}, \overline{\mathcal{C}}_{\mathcal{A},2}, \overline{\mathcal{C}}_{L,1}\} - \mathcal{R}'$ reduces to $\approx 0$ at high SNR. Based on these numerical observations, we state the following corollary.

*Corollary 2:* The input distribution $\tilde{g}_{\mu,\nu}(x)$ is nearly capacity achieving (i.e., the gap to capacity is $\approx 0$) at high SNR.

Since we are often interested in simple capacity characterizations, we approximate the high SNR capacity by

$$\mathcal{C}_{\text{high SNR}} = \lim_{\gamma \to \infty} \min\{\overline{\mathcal{C}}_{\mathcal{E}}, \overline{\mathcal{C}}_{\mathcal{A},2}\} = \min\left\{\frac{1}{2}\log\left(\frac{e\bar{\gamma}^2}{2\pi}\right), \frac{1}{2}\log\left(\frac{\gamma^2}{2\pi e}\right)\right\},$$

as in Proposition 1. This approximation is exact for $\frac{\mathcal{E}}{\mathcal{A}} > \frac{1}{2}$ at high SNR where the lower bound [9, (18)] coincides with $\overline{\mathcal{C}}_{\mathcal{A},2}$. This approximation is nearly tight ($\approx 0$ gap to capacity) for $\frac{\mathcal{E}}{\mathcal{A}} \leq 0.15$ where $\mathcal{R}'$ approaches $\overline{\mathcal{C}}_{\mathcal{E}}$ (see Fig. 2a). For $0.15 < \frac{\mathcal{E}}{\mathcal{A}} \leq \frac{1}{2}$, the approximation is fairly tight since the gap is $< 0.1$ nats and can be neglected at high SNR.

## VII. Capacity Fitting

It is of practical interest to have a capacity lower bound which has a closed-form. Such an expression can be used to study power allocation and outage/ergodic capacities of fading scenarios. While such a closed form expression is given for high SNR by Proposition 1, and for low SNR by [9], it is not available for moderate SNR which is the regime of operation of practical systems. With this in mind, we provide a simple expression for the achievable rate in an IM-DD channel using curve-fitting.

### A. Global Fitting

We first present a global fitting for the capacity of the channel for all SNR. This requires choosing the fitting function carefully to capture the behavior of the capacity from low to high SNR.

Let the fitting function be denoted $\Psi(\gamma)$. As discussed in the previous section, the high SNR capacity of the channel scales as $\frac{1}{2}\log(c_1\gamma^2)$ for some $c_1 > 0$. On the other hand, the low SNR capacity scales as $c_2\frac{\gamma^2}{2}$ [9] for some $c_2 > 0$. A suitable fitting for high and low $\gamma$ is thus given by the function $\Psi(\gamma) = \frac{1}{2}\log\left(1 + \gamma^2(c_1 + (c_2 - c_1)\Theta(\gamma))\right)$,

where $\Theta(\gamma)$ is a function which satisfies $\lim_{\gamma\to\infty}\Theta(\gamma)=0$ and $\lim_{\gamma\to 0}\Theta(\gamma)=1$. By choosing $c_1$ and $c_2$ appropriately, $\Psi(\gamma)$ captures the high and low SNR behavior of capacity. It remains to capture the achievable rates in the moderate SNR regime. Achievable rates for this regime can be obtained from [10], based on a discrete distribution on $X$ (see Figure 3). To capture these rates, we have to choose $\Theta(\gamma)$ appropriately. A suitable choice is of the form of a $\Theta(\gamma)=\frac{\Theta_1(\gamma)}{\Theta_2(\gamma)}$, where $\Theta_1(\gamma)$ and $\Theta_2(\gamma)$ are polynomials of degrees $m_1$ and $m_2$ in $\gamma$, respectively, with $m_1<m_2$. That is,

$$\Psi(\gamma)=\frac{1}{2}\log\left(1+\gamma^2\left(c_1+(c_2-c_1)\frac{\sum_{k=0}^{m_1}a_k\gamma^k}{\sum_{k=0}^{m_2}b_k\gamma^k}\right)\right),$$

for some $c_1$, $c_2$, $a_k$ and $b_k$ to be determined. Without loss of generality, we fix $a_0=b_0=1$. The remaining coefficients of have to be chosen so that $\Theta_1(\gamma)$ and $\Theta_2(\gamma)$ have no roots in $[0,\infty)$ to avoid singularities.

The parameters $c_1$ and $c_2$ can be easily fixed using our knowledge of the high and low SNR capacity of the channel. Namely,

$$c_1=\min\left\{\frac{e\bar{\gamma}^2}{2\pi\gamma^2},\frac{1}{2\pi e}\right\}, \tag{35}$$

$$c_2=\min\left\{\frac{\bar{\gamma}}{\gamma}\left(1-\frac{\bar{\gamma}}{\gamma}\right),\frac{1}{4}\right\}. \tag{36}$$

The parameters $m_1$ and $m_2$ can be chosen based on the number of SNR-Rate pairs $(\gamma,R)$ used for the fitting in the moderate SNR regime. In particular, given $N_p$ such pairs $\{(\gamma_1,R_1),\cdots,(\gamma_{N_p},R_{N_p})\}$, we can choose $m_2=\left\lceil\frac{N_p+1}{2}\right\rceil$ and $m_1=N_p-m_2$. This guarantees that $m_1<m_2$ and that the number of unknown parameters of the fitting function $\Psi(\gamma)$ does not exceed $N_p$. After fixing $m_1$ and $m_2$, the parameters $a_k$ and $b_k$ can be easily chosen by solving the linear system of equations

$$\sum_{k=0}^{m_1}a_k\gamma_i^k-\left(\frac{e^{2R_i}-1-c_1\gamma_i^2}{(c_2-c_1)\gamma_i^2}\right)\sum_{k=0}^{m_2}b_k\gamma_i^k=0,\quad i=1,\cdots,N_p. \tag{37}$$

Thus, by choosing $m_1$ and $m_2$ as described above, we have $N_p$ equations with $N_p$ unknowns and we can solve for the parameters $a_k$ and $b_k$.

By numerical inspection of the fitting, a very close fit can be obtained for $N_p\leq 3$ (see Fig. 10). By using $N_p=1$ and $N_p=3$, we get $(m_1,m_2)=(0,1)$ and $(m_1,m_2)=(1,2)$. While the latter gives a very close fit, the former gives a simpler fitting function at the expense of a small gap. The coefficients of the fitting functions are summarized in Table III for different values of $\frac{\mathcal{E}}{\mathcal{A}}$. For the five cases in this table, the polynomials $\Theta_1(\gamma)$ and $\Theta_2(\gamma)$ have no roots in $[0,\infty)$. Notice that the achievable rate (as a function of $\gamma$) of an IM-DD channel with a given $\frac{\mathcal{E}}{\mathcal{A}}$ is also achievable for any channel with larger $\frac{\mathcal{E}}{\mathcal{A}}$, since the latter has larger average constraint. Thus, by plugging the coefficients given in III for $\frac{\mathcal{E}}{\mathcal{A}}=\alpha$ in $\Psi(\gamma)$, we obtain achievable rates for an IM-DD with $\frac{\mathcal{E}}{\mathcal{A}}>\alpha$ as well. The values in the table can be used for studying the performance of fading IM-DD channels at any SNR.

### *B. Local Fitting*

The fitting function $\Psi(\gamma)$ is a close fit for all SNR. However, in practice, we are often interested in functions of the form $\frac{1}{2}\log(1+c\gamma^2)$, especially since numerous techniques have been developed over the time to study capacity of this form in fading scenarios (power allocation, outage, etc.) [27], [28]. Thus, it is natural to seek a fitting function of this form. Next, we simplify the fitting function $\Psi(\gamma)$ to this form by sacrificing its global tightness.

| $\frac{\mathcal{E}}{\mathcal{A}}$ | | 0.1 | 0.2 | 0.3 | 0.4 | 0.5 |
|---|---|---|---|---|---|---|
| $N_p = 1$ | $a_0$ | 1 | 1 | 1 | 1 | 1 |
| | $(b_0, b_1)$ | $(1, 0.47)$ | $(1, 0.43)$ | $(1, 0.56)$ | $(1, 0.8)$ | $(1, 0.41)$ |
| $N_p = 3$ | $(a_0, a_1)$ | $(1, 0.38)$ | $(1, 0.45)$ | $(1, 0.14)$ | $(1, 0.05)$ | $(1, 0.57)$ |
| | $(b_0, b_1, b_2)$ | $(1, 0.19, 0.2)$ | $(1, 0.24, 0.21)$ | $(1, 0.04, 0.1)$ | $(1, -0.03, 0.07)$ | $(1, 0.32, 0.26)$ |

TABLE III: Coefficients of the fitting function $\Psi(\gamma)$ using one fitting point at $\gamma = 15$ dB and three fitting points at $\gamma \in \{0, 10, 15\}$ dB.

As evident from Fig. 3 e.g., the lower bound $\mathcal{R}_F$ can not be captured by a function of the form $\frac{1}{2}\log(1 + c\gamma^2)$ in the moderate $\gamma$ regime since this function has a larger pre-log. However, a local fit can be obtained by using a rather simple fitting function

$$\widehat{\Psi}(\gamma) = \frac{d_1}{2}\log(1 + d_2\gamma^2),$$

where $d_1$ and $d_2$ are positive scalars. Clearly, at high $\gamma$, $d_1 = 1$ and $d_2 = c_1$ given in (35). At low $\gamma$, we can choose any $d_1$ and $d_2$ such that $d_1 d_2 = c_2$ given in (36). This provides a good fit at high and low SNR. For moderate SNR, $d_1$ and $d_2$ have to be chosen to reduce the gap between $\widehat{\Psi}(\gamma)$ and the achievable rate $\mathcal{R}_F$ for an SNR range of interest. It is also important to maintain $\hat{\Psi}(\gamma) < \mathcal{R}_F$ to guarantee that $\hat{\Psi}(\gamma)$ is achievable. Next, we propose a simple method to obtain a local fit for moderate $\gamma$.

Consider an SNR range of interest given by $\gamma \in [\gamma_1, \gamma_2]$ dB for some $\gamma_1$ and $\gamma_2$, and consider the achievable rates $R_1$, $R_2$, and $R_0$ corresponding to $\mathcal{R}_F$ in [10] at $\gamma_1$, $\gamma_2$, and some $\gamma_0 \in [\gamma_1, \gamma_2]$, respectively. First, we choose $d_1$ as the pre-log of $\mathcal{R}_F$ (slope with respect to $\log(\gamma)$) in this range of $\gamma$, i.e., $d_1 = \frac{R_2 - R_1}{\log(\gamma_2) - \log(\gamma_1)}$. Roughly speaking, this indicates that the achievable rate $\mathcal{R}_F$ scales as $d_1 \log(\gamma) = \frac{d_1}{2}\log(\gamma^2)$ in this range. Now, to fix $d_2$, we equate $\widehat{\Psi}(\gamma_0)$ to $R_0$, leading to $d_2 = \frac{e^{\frac{2R_0}{d_1}} - 1}{\gamma_0^2}$.

Alternatively, one could use an MMSE approach to minimize the gap between $\hat{\Psi}(\gamma)$ and $\mathcal{R}_F$. We repeat that $\widehat{\Psi}(\gamma)$ provides local fitting, contrary to $\Psi(\gamma)$. The behavior of $\widehat{\Psi}(\gamma)$ is depicted in Figure 10. Note that $\widehat{\Psi}(\gamma)$ provides a good fit for the range of interest. The advantage of this function is that it has a simple form that can be used for studying fading scenarios using existing tools. In scenarios with weak turbulence conditions, the SNR $\gamma$ does not vary widely resulting in a distribution of $\gamma$ that is thin around a nominal value $\gamma_0$. The performance of a system operating around $\gamma_0$ can be well described by $\widehat{\Psi}(\gamma)$ in the given range.

## VIII. IM-DD vs. Heterodyne

In free-space optical communication, heterodyne detection can be used instead of IM-DD. Although HD can achieve higher rates than IM-DD, it is significantly more complicated and more expensive. The advantage of HD is that it allows amplitude and phase modulation. Whether it is beneficial to deploy HD or not is determined by the gain attained by this deployment, in comparison with the additional cost. Thus, it is interesting to compare the achievable rates of the two systems, and quantify their difference.

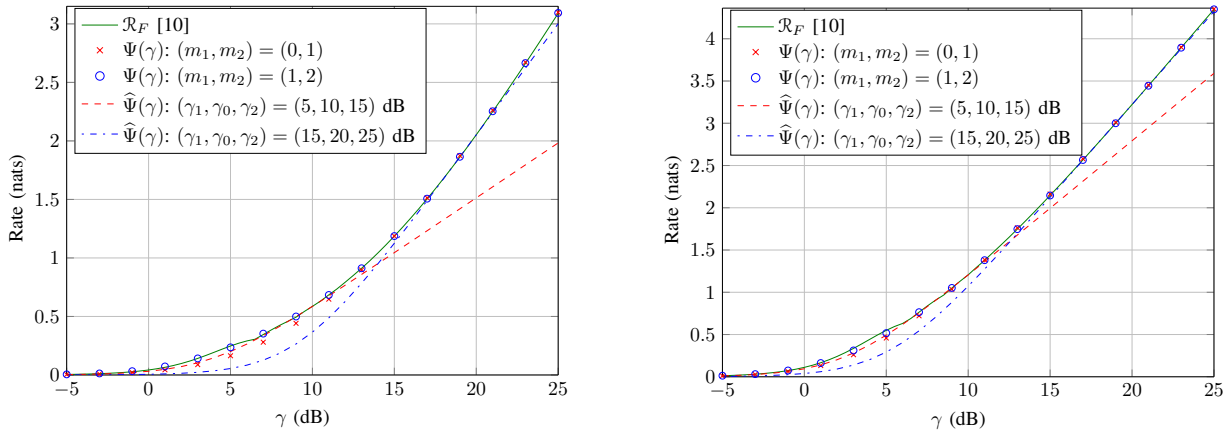


(a) $\frac{\mathcal{E}}{\mathcal{A}} = 0.1$.

(b) $\frac{\mathcal{E}}{\mathcal{A}} = \frac{1}{2}$.

Fig. 10: Global and local fitting of the achievable rate $\mathcal{R}_F$ using $\Psi(\gamma)$ and $\widehat{\Psi}(\gamma)$.

### *A. Heterodyne Detection*

The optical heterodyne receiver is described in detail in [13]. The main idea is mixing the optical signal with an optical local oscillator (LO) to convert the optical signal to a lower intermediate frequency where detection takes place.

*1) Model:* Let the optical signal be given by $a\cos(\omega t)$ where $a$ is the modulated amplitude, and $\omega$ is the frequency of the optical signal. Also, let the LO signal be given by $a_0\cos(\omega_0 t)$ where $a_0$ and $\omega_0$ are constants. Denote the powers of these two signals by $P = a^2/2$ and $P_0 = a_0^2/2$. The detected current after mixing the two signals is given by $i_x = \rho a a_0 \cos((\omega_0 - \omega)t)$ where $\rho$ is a constant dependent on the efficiency of the detector among other parameters.

The corresponding detected signal power is $2\rho^2 P P_0$ (load resistance 1 Ohm). This operation induces a noise current $i_z$ composed of shot-noise and thermal noise. The shot-noise can be assumed to be Gaussian[5] and has variance $2qBI$ where $q$ is the electron charge, $B$ is the bandwidth, and $I$ is the sum of all shot-noise induced currents [29]. This current is $I = \rho(P_0 + P + P_b)$ where $P_b$ is the power of the background radiation. Adding thermal noise of variance $\sigma_{\text{th}}^2$ leads to an overall noise of variance $2qB\rho(P_0 + P) + (2qB\rho P_b + \sigma_{\text{th}}^2)$. We combine the background noise and the thermal noise to one noise with variance $\rho^2\sigma_1^2$ where

$$\sigma_1^2 = \frac{2qBP_b}{\rho} + \frac{\sigma_{\text{th}}^2}{\rho^2}.$$

The resulting electrical signal-to-noise ratio (ESNR) is $\gamma_{\text{HD}}^e(P) = \frac{2PP_0}{\sigma_2^2(P_0+P)+\sigma_1^2}$ where we used

$$\sigma_2^2 = \frac{2qB}{\rho}.$$

[5]if the symbol duration is large enough in comparison to the rate of photon arrivals

Note that increasing the power of the LO signal $P_0$ increases the ESNR and makes the LO shot-noise dominate all other noise sources, leading to an ESNR of

$$\gamma^{e}_{\text{HD}}(P) = \frac{2P}{\sigma_2^2}.$$

Furthermore, this noise can be approximated by a Gaussian distribution. Both signal amplitude and phase can be retrieved from the detected signal. Thus, the channel in this case can thus be modeled as a complex Gaussian channel with an ESNR of $\gamma^{e}_{\text{HD}}(P)$. In other words, the HD channel can be modeled by $Y = X + Z$ where $X \in \mathbb{C}$ has power $P$ and $Z$ is complex Gaussian with mean $0$ and variance $\sigma_2^2/2$.

*2) Capacity and Capacity Bounds:* Consider an HD channel with a peak intensity constraint $\mathcal{A}$, i.e., $|X| \leq \sqrt{\mathcal{A}}$ and noise variance $\sigma_2^2/2$. The capacity of this *complex* Gaussian channel can be upper bounded by twice that of a *real* Gaussian channel with peak constraint $\mathcal{A}$ and noise variance $\sigma_2^2/4$ [30]. The high-SNR capacity of the *real* Gaussian channel with a peak constraint has been given by Shannon in [31]. For a *real* Gaussian channel with a peak constraint $\mathcal{A}$ and noise variance $\sigma_2^2/4$, the high-SNR capacity is $\frac{1}{2}\log\left(1+\frac{8\mathcal{A}}{\pi e\sigma_2^2}\right)$. Thus, the capacity $\mathcal{C}_{HD,\mathcal{A}}$ of the HD system with a peak constraint satisfies

$$\mathcal{C}_{\text{HD},\mathcal{A}} \leq \overline{\mathcal{C}}_{\text{HD},\mathcal{A}} = \log\left(1+\frac{8\mathcal{A}}{\pi e\sigma_2^2}\right). \tag{38}$$

Under an average constraint $\mathcal{E}$, we have $\mathbb{E}[|X|^2] \leq \mathcal{E}$. The capacity $\mathcal{C}_{\text{HD},\mathcal{E}}$ of the HD system in this case is given by [31]

$$\mathcal{C}_{\text{HD},\mathcal{E}} = \log\left(1+\frac{2\mathcal{E}}{\sigma_2^2}\right). \tag{39}$$

We are also interested in a comparison between IM-DD and a HD system employing pulse-amplitude modulation (PAM) which we call HD-PAM. The reason for this comparison is that both IM-DD and HD-PAM employ real signaling, contrary to HD which is capable of employing complex signaling. The high-SNR capacity of an HD-PAM system under a peak constraint $\mathcal{A}$ is given by [31]

$$\hat{\mathcal{C}}_{\text{HD},\mathcal{A}} = \frac{1}{2}\log\left(1+\frac{8\mathcal{A}}{\pi e\sigma_2^2}\right). \tag{40}$$

Under an average constraint $\mathcal{E}$, this system has a capacity of [31]

$$\hat{\mathcal{C}}_{\text{HD},\mathcal{E}} = \frac{1}{2}\log\left(1+\frac{4\mathcal{E}}{\sigma_2^2}\right), \tag{41}$$

where the factor $4$ arises since only the real-valued noise affects the HD-PAM system. The expressions $\overline{\mathcal{C}}_{\text{HD},\mathcal{A}}$, $\mathcal{C}_{\text{HD},\mathcal{E}}$, $\hat{\mathcal{C}}_{\text{HD},\mathcal{A}}$, and $\hat{\mathcal{C}}_{\text{HD},\mathcal{E}}$ will be used for comparison with IM-DD next.

### *B. IM-DD*

*1) Input-dependent Noise Model:* On the other hand, consider an IM-DD system with an optical signal $a\cos(\omega t)$ as above. This signal is detected by a detection device (photodiode e.g.), after which the detected current is $i_x = \rho a^2/2 = \rho P$ and the corresponding power $\rho^2 P^2$. Similar to the HD system, this process induces a noise current $\tilde{i}_z$ consisting of shot-noise and thermal noise. This noise is Gaussian with variance $\tilde{\sigma}_z^2 = \sigma_2^2\rho^2 P + \rho^2\sigma_1^2$. Thus, the channel can be modeled by a Gaussian channel with input-dependent noise with output $\tilde{Y} = X + \sqrt{X}Z_2 + Z_1$

[16], where $X = P \in \mathbb{R}_+$, and $Z_1$ and $Z_2$ are real Gaussian noises with variances $\sigma_1^2$ and $\sigma_2^2$, respectively. Note that the noise is dependent on $X$. Note that a peak intensity constraint in this case means $X \leq \mathcal{A}$, and an average intensity constraint means $\mathbb{E}[X] \leq \mathcal{E}$.

We would like to use the simple high SNR capacity approximation of the IM-DD channel given in Proposition 1. However, this approximation applies for an IM-DD channel with input-independent noise. Next, we prove a result which lower bounds the capacity of an IM-DD channel with input-dependent noise at high SNR by that of an IM-DD channel with input-independent noise.

*2) Capacity Bounds:* At high SNR, the following lemma holds.

*Lemma 2:* At high SNR, the capacity of the IM-DD channel with input $X$ and output $\tilde{Y} = X + \sqrt{X}Z_2 + Z_1$, where $X \in \mathbb{R}_+$, $X \leq \mathcal{A}$, $\mathbb{E}[X] \leq \mathcal{E}$, and $Z_1$ and $Z_2$ are independent Gaussian noises with variances $\sigma_1^2$ and $\sigma_2^2$ is lower bounded by the capacity of an IM-DD channel with input $X$ satisfying the same constraints, and output $Y = X + Z$ where $Z$ is Gaussian with variance $\sigma^2 = \sigma_2^2 \min\{\mathcal{E}, \frac{\mathcal{A}}{2}\} + \sigma_1^2$.

*Proof:* The channel capacity $\tilde{\mathcal{C}}$ is given by

$$\tilde{\mathcal{C}} = \max_{f(x) \in \mathcal{F}} I(X; \tilde{Y}) \tag{42}$$

$$\geq \max_{f(x) \in \mathcal{F}_{\tilde{g}}} I(X, \tilde{Y}), \tag{43}$$

where $\mathcal{F}$ is the set of distributions of $X \in [0, \mathcal{A}]$ with $\mathbb{E}[X] \leq \mathcal{E}$, and $\mathcal{F}_{\tilde{g}}$ is the set of truncated-Gaussian distributions $\tilde{g}_{\mu,\nu}(x)$ as defined in Section VI-B, satisfying $\mathcal{F}_{\tilde{g}} \subset \mathcal{F}$ and $\mathbb{E}[X] = \min\{\mathcal{E}, \frac{\mathcal{A}}{2}\}$. Thus, we can write

$$\max_{f(x) \in \mathcal{F}} I(X; \tilde{Y}) \geq h(X_{\tilde{g}_{\mu,\nu}}) - h(X_{\tilde{g}_{\mu,\nu}} | \tilde{Y}), \tag{44}$$

where $X_{\tilde{g}_{\mu,\nu}} \sim \tilde{g}_{\mu,\nu}(x) \in \mathcal{F}_{\tilde{g}}$ with variance $\tilde{\nu}^2 = \nu^2(1 - (\mathcal{A} - \mu)\tilde{g}_{\mu,\nu}(\mathcal{A}) - \mu\tilde{g}_{\mu,\nu}(0) - \nu^2(\tilde{g}_{\mu,\nu}(0) - \tilde{g}_{\mu,\nu}(\mathcal{A}))^2)$ (can be derived similar to (97)-(100) in Appendix E) and mean $\tilde{\mu}$ (31). The entropy of $X_{\tilde{g}_{\mu,\nu}}$ is given by

$$h(X_{\tilde{g}_{\mu,\nu}}) = \frac{1}{2}\log(2\pi e \nu^2) - \log(\eta) - \frac{1}{2}\left((\mathcal{A} - \mu)\tilde{g}_{\mu,\nu}(\mathcal{A}) + \mu\tilde{g}_{\mu,\nu}(0)\right). \tag{45}$$

On the other hand, $h(X_{\tilde{g}_{\mu,\nu}} | \tilde{Y})$ can be bounded as follows

$$h(X_{\tilde{g}_{\mu,\nu}} | \tilde{Y}) \leq \max_{f(x) \in \mathcal{F}'} h(X | \tilde{Y}), \tag{46}$$

where $\mathcal{F}'$ is the set of distributions of $X \in \mathbb{R}$ satisfying $\mathbb{E}[X] = \min\{\mathcal{E}, \frac{\mathcal{A}}{2}\}$ and $\text{Var}(X) = v \leq \tilde{\nu}^2$, and where the inequality follows since $\tilde{g}_{\mu,\nu}(x) \in \mathcal{F}'$. Note that under a given covariance matrix $Q = \left[\begin{smallmatrix} q_{11} & q_{12} \\ q_{21} & q_{22} \end{smallmatrix}\right]$ of $(X, \tilde{Y})$, the conditional entropy $h(X|\tilde{Y})$ is maximized if the pair $(X, \tilde{Y})$ is Gaussian distributed [32], and the maximum is $\frac{1}{2}\log(2\pi e|Q|/q_{22})$. Let us find $Q$ for $f(x) \in \mathcal{F}'$. We have

$$\mathbb{E}[(X - \mathbb{E}[X])^2] = v \tag{47}$$

$$\mathbb{E}[(X - \mathbb{E}[X])(\tilde{Y} - \mathbb{E}[\tilde{Y}])] = v \tag{48}$$

$$\mathbb{E}[(\tilde{Y} - \mathbb{E}[\tilde{Y}])^2] = v + \sigma_2^2\mathbb{E}[X] + \sigma_1^2. \tag{49}$$

Since $f(x) \in \mathcal{F}' \Rightarrow \mathbb{E}[X] = \min\{\mathcal{E}, \frac{\mathcal{A}}{2}\}$, then $Q = \left[\begin{smallmatrix} v & v \\ v & v+\sigma^2 \end{smallmatrix}\right]$ where $\sigma^2 = \sigma_2^2 \min\{\mathcal{E}, \frac{\mathcal{A}}{2}\} + \sigma_1^2$. Therefore, we have

$$\max_{f(x)\in\mathcal{F}'} h(X|\tilde{Y}) \leq \max_{v\in[0,\tilde{\nu}^2]} \frac{1}{2}\log\left(2\pi e \frac{v\sigma^2}{v+\sigma^2}\right) \tag{50}$$

$$= \frac{1}{2}\log\left(2\pi e \frac{\tilde{\nu}^2\sigma^2}{\tilde{\nu}^2+\sigma^2}\right). \tag{51}$$

Since $\tilde{\mu} = \min\{\mathcal{E}, \frac{\mathcal{A}}{2}\}$, then $\mu \leq \tilde{\mu}$, $\tilde{g}_{\mu,\nu}(0) - \tilde{g}_{\mu,\nu}(\mathcal{A}) \geq 0$, and hence $\tilde{\nu}^2 \leq \nu^2$. Therefore,

$$\tilde{\mathcal{C}} \geq \frac{1}{2}\log\left(1+\frac{\nu^2}{\sigma^2}\right) - \log(\eta) - \frac{1}{2}\left((\mathcal{A}-\mu)\tilde{g}_{\mu,\nu}(\mathcal{A}) + \mu\tilde{g}_{\mu,\nu}(0)\right). \tag{52}$$

But this lower bound coincides with $\mathcal{R}'$ in Theorem 4 at high SNR.[6] But $\mathcal{R}'$ nearly coincides with the capacity of the channel $Y = X + Z$ where $Z$ is Gaussian with variance $\sigma^2$ at high SNR (Fig. 2b). We conclude that $\tilde{\mathcal{C}}$ is lower bounded by the capacity of an IM-DD channel with input-independent noise whose variance is $\sigma^2$ at high SNR. This proves the statement of the lemma. ■

*3) Cost-dependent Noise Model:* Based on Lemma 2, we propose the following model.

*Definition 1 (IM-DD Channel with Cost-dependent Gaussian Noise):* An IM-DD channel with cost-dependent Gaussian noise is a channel $Y = X + Z$ where $X \in [0, \mathcal{A}]$ and $\mathbb{E}[X] \leq \mathcal{E}$, and where $Z \sim g_{0,\sigma}(z)$ with $\sigma^2 = \sigma_2^2 \min\{\mathcal{E}, \frac{\mathcal{A}}{2}\} + \sigma_1^2$ for some $\sigma_1^2, \sigma_2^2$.

This model combines the properties of [9]–[11] since its noise is input-independent, and [16] since it captures the increasing impact of shot-noise at high SNR.

Note that the input-independent noise model which ignores the input-dependent noise component, has noise variance $\sigma^2$ independent of $X$, $\mathcal{A}$, and $\mathcal{E}$. This model is convenient to deal with, but it leads to an overestimation of the high SNR capacity scaling. On the other hand, the input-dependent noise model in [16] captures the high SNR capacity scaling, but its analysis is more complicated. The cost-dependent noise model bridges the two models.

At high SNR, the cost-dependent noise has variance $\sigma^2 = \sigma_2^2 \min\{\mathcal{E}, \frac{\mathcal{A}}{2}\} + \sigma_1^2$ which approaches $\sigma_2^2 \min\{\mathcal{E}, \frac{\mathcal{A}}{2}\}$. Using Proposition 1 in conjunction with this cost-dependent noise leads to the high SNR capacity lower bound

$$\tilde{\mathcal{C}}_{\text{High SNR}} \geq \underline{\tilde{\mathcal{C}}} = \begin{cases} \frac{1}{2}\log\left(\frac{e\mathcal{E}}{2\pi\sigma_2^2}\right) & \frac{\mathcal{E}}{\mathcal{A}} < 0.15 \\ \frac{1}{2}\log\left(\frac{e\mathcal{E}}{2\pi\sigma_2^2}\right) - 0.1 & 0.15 \leq \frac{\mathcal{E}}{\mathcal{A}} < \frac{1}{e} \\ \frac{1}{2}\log\left(\frac{\mathcal{A}^2}{2\pi e\sigma_2^2\mathcal{E}}\right) - 0.1 & \frac{1}{e} \leq \frac{\mathcal{E}}{\mathcal{A}} < \frac{1}{2} \\ \frac{1}{2}\log\left(\frac{\mathcal{A}}{\pi e\sigma_2^2}\right) & \frac{1}{2} \leq \frac{\mathcal{E}}{\mathcal{A}} \end{cases}$$

This has the same scaling as the high SNR capacity of the IM-DD channel with input-dependent noise given in [16]. The additional $0.1$ nats arises since the approximation in Proposition 1 has a gap of $0.1$ nats to capacity at high SNR in the range $0.15 \leq \frac{\mathcal{E}}{\mathcal{A}} < \frac{1}{2}$. Next, we use this capacity lower bound $\underline{\tilde{\mathcal{C}}}$ for comparison with HD.

[6]At high SNR where $\mathcal{E}, \mathcal{A} \gg \sigma$, the optimal $\nu$ also satisfies $\nu \gg \sigma$.

### C. Comparison

*1) Peak Constraint:* Under a peak constraint only, we have

$$\mathcal{C}_{\text{HD},\mathcal{A}} - \tilde{\mathcal{C}}_{\text{High SNR}} \leq \overline{\mathcal{C}}_{\text{HD},\mathcal{A}} - \underline{\tilde{\mathcal{C}}} \tag{53}$$

$$\approx \log(\delta_1) \tag{54}$$

where $\delta_1 = \frac{8\sqrt{\mathcal{A}}}{\sqrt{\pi e}\sigma_2}$. This implies that, under the same constraints, HD achieves at most $\log(\delta_1)$ nats more than IM-DD. Equivalently, IM-DD requires at most $10\log_{10}(\delta_1)$ dB more SNR than HD to achieve the same rate (with respect to the HD SNR). Note that the gap increases with SNR due to the fact that HD allows 2-dimensional modulation (amplitude and phase), while IM-DD is restricted to one dimension (intensity).

For a fairer comparison, we compare IM-DD with HD-PAM. In this case, we have

$$\hat{\mathcal{C}}_{\text{HD},\mathcal{A}} - \tilde{\mathcal{C}}_{\text{High SNR}} \leq \hat{\mathcal{C}}_{\text{HD},\mathcal{A}} - \underline{\tilde{\mathcal{C}}} \tag{55}$$

$$\approx \log(\sqrt{8}) \tag{56}$$

Consequently, HD-PAM achieves at most $\log(\sqrt{8}) \approx 1.04$ nats ($1.5$ bits) more than IM-DD, or equivalently, requires $10\log_{10}(\sqrt{8}) \approx 4.52$ dB less SNR. This leads to the results in the first row of Table I.

*2) Average Constraint:* Under an average optical intensity constraint $\mathcal{E}$, we have

$$\mathcal{C}_{\text{HD},\mathcal{E}} - \tilde{\mathcal{C}}_{\text{High SNR}} \leq \mathcal{C}_{\text{HD},\mathcal{E}} - \underline{\tilde{\mathcal{C}}} \tag{57}$$

$$\approx \log(\delta_2) \tag{58}$$

where $\delta_2 = \frac{\sqrt{8\pi\mathcal{E}}}{\sqrt{e}\sigma_2}$. Thus, HD achieves at most $\log(\delta_2)$ nats more than IM-DD at the same $\mathcal{E}$, or equivalently, IM-DD requires at most $10\log_{10}(\delta_2)$ dB more SNR than HD to achieve the same rate (with respect to HD SNR).

If we restrict HD to PAM, then we have

$$\hat{\mathcal{C}}_{\text{HD},\mathcal{E}} - \tilde{\mathcal{C}}_{\text{High SNR}} \leq \hat{\mathcal{C}}_{\text{HD},\mathcal{E}} - \underline{\tilde{\mathcal{C}}} \tag{59}$$

$$\approx \log(\sqrt{8\pi/e}) \tag{60}$$

Consequently, HD-PAM achieves at most $1.11$ nats ($1.6$ bits) more than IM-DD at the same $\mathcal{E}$, or equivalently, requires $\approx 4.83$ dB less SNR to achieve the same rate. This leads to the results in the last row of Table I.

*3) Average and Peak Constraints:* In this case, the capacity of the HD system can be upper bounded by the capacities under either an average or a peak constraint, i.e.,

$$C_{\text{HD}} \leq \min\left\{\overline{C}_{\text{HD},\mathcal{A}}, C_{\text{HD},\mathcal{E}}\right\}, \tag{61}$$

$$\hat{C}_{\text{HD}} \leq \min\left\{\hat{C}_{\text{HD},\mathcal{A}}, \hat{C}_{\text{HD},\mathcal{E}}\right\}, \tag{62}$$

where $C_{\text{HD}}$ and $\hat{C}_{\text{HD}}$ are the capacities of the HD and HD-PAM systems under both average and peak constraints, respectively. For IM-DD, the capacity is bounded by $\underline{\tilde{\mathcal{C}}}$.

For $\frac{\mathcal{E}}{\mathcal{A}} > \frac{1}{2}$, comparing $\underline{\tilde{\mathcal{C}}}$ with $\overline{C}_{\text{HD},\mathcal{A}}$ and $\hat{C}_{\text{HD},\mathcal{A}}$ yields the same gap as for the case under a peak constraint only as given in the first row of Table I.

For $\frac{\mathcal{E}}{\mathcal{A}} \leq \frac{1}{2}$, we have two cases. If $\frac{\mathcal{E}}{\mathcal{A}} \geq \frac{1}{e}$, then we have

$$\underline{\tilde{\mathcal{C}}} = \log\left(\frac{\mathcal{A}}{\sqrt{2\pi e\mathcal{E}}\sigma_2}\right) - 0.1 \geq \log\left(\frac{\sqrt{\mathcal{A}}}{\sqrt{\pi e}\sigma_2}\right) - 0.1 \tag{63}$$

since $\frac{\mathcal{E}}{\mathcal{A}} \leq \frac{1}{2}$. By comparing with $\overline{C}_{\text{HD},\mathcal{A}}$ and $\hat{C}_{\text{HD},\mathcal{A}}$, we obtain the same gaps as for the case $\frac{\mathcal{E}}{\mathcal{A}} > \frac{1}{2}$, with an additional gap of $0.1$ nats ($0.145$ bits) or $0.43$ dB. This additional gap is negligible with respect to the gap between HD and IM-DD, and increases the capacity gap between HD-PAM and IM-DD to $1.14$ nats ($1.645$ bits) or equivalently $4.95$ dB as given in the second row of Table I.

Otherwise, if $\frac{\mathcal{E}}{\mathcal{A}} < \frac{1}{e}$, then by comparing with $C_{\text{HD},\mathcal{E}}$ and $\hat{C}_{\text{HD},\mathcal{E}}$, we obtain the same gaps as for the case under an average constraint only, plus and additional gap of $0.1$ nats for $0.15 < \frac{\mathcal{E}}{\mathcal{A}} \leq \frac{1}{2}$. This does not affect the gap between HD and IM-DD since it can be neglected, and increases the gap between HD-PAM and IM-DD to $1.21$ nats ($1.745$ bits) or $5.26$ dB as given in the third row of Table I.

## IX. Conclusion

We studied a simple model of the IM-DD channel with input-independent noise. For this model, we proposed a new approach for deriving sphere-packing upper bounds. The proposed recursive approach is better than the approach that uses the Steiner-Minkowski formula which is commonly used in literature. The main reason is that our approach makes use of the geometry of the ball, while the other approach does not. This recursive approach can in fact be applied to any scenario where the input signal of the channel is confined to a polyhedron. The resulting bounds are tighter than existing bounds in some SNR regimes. An interesting extension of these sphere-packing bounds would be to generalize them to the intersection of a cube and a simplex, which better captures the IM-DD channel under both average and peak intensity constraints. We also derived the rate achieved by using a truncated-Gaussian input distribution. By comparing with the upper bounds, we show that the gap between the achievable rate and upper bounds is negligible at high SNR. We also provide simple functions that describe the highest known achievable rate of this channel globally and locally. Such function can be of great importance for studying fading in practical systems.

Finally, we compared the performance of heterodyne detection and IM-DD at high SNR, and bounded the gap between the two systems. For this comparison, we define a new cost-dependent channel model, which captures the high and low SNR behavior of the channel. This model is motivated by a result proving that, at high SNR, the capacity of an IM-DD channel with input-dependent noise is lower bounded by that of an IM-DD channel with input-independent noise whose variance depends on the input cost instead of the input itself. This model converges to the input-independent Gaussian IM-DD commonly studied in literature at low SNR, and captures the high SNR scaling of the IM-DD with input-dependent noise at high SNR. Furthermore, since this model falls under the class of the input-independent Gaussian IM-DD, all existing results on this channel can be applied to our model.

## Appendix A
## Sufficiency of $\mathbb{E}[X] = \min\{\mathcal{E}, \frac{\mathcal{A}}{2}\}$

Here we show that for an IM-DD channel with input-independent noise, the capacity achieving input distribution satisfies $\mathbb{E}[X] = \min\{\mathcal{E}, \frac{\mathcal{A}}{2}\}$. This is in particular useful for channels with a peak constraint since under an average

constraint only ($\mathcal{A} = \infty$), we can always shift $X$ to obtain a distribution with a larger mean achieving the same rate. This follows from the invariance of mutual information to shifts in the input distribution. Thus, it is sufficient to choose $\mathbb{E}[X] = \mathcal{E}$ in this case.

While this can be applied for channels with an average constraint only, this is in general not possible for $X \in [0, \mathcal{A}]$ since shifting might lead to an infeasible distribution. Instead of using this property, we show next that over the set of distributions of $X \in [0, \mathcal{A}]$, $\mathcal{C}$ is increasing in $\mathbb{E}[X]$ for $\mathbb{E}[X] \in (0, \frac{\mathcal{A}}{2}]$, and decreasing for $\mathbb{E}[X] \in (\frac{\mathcal{A}}{2}, \mathcal{A}]$.

The proof is similar to [9, Proposition 9]. Consider a peak constrained IM-DD channel, and an input distributions $f_1(x)$ and $f_2(x)$ on $X \in [0, \mathcal{A}]$ with means $\mu_1 \leq \frac{\mathcal{A}}{2}$ and $\mu_2 \geq \frac{\mathcal{A}}{2}$, respectively, where $f_2(x) = f_1(\mathcal{A} - x)$. The rates achieved by these distributions are denoted $I_1$ and $I_2$, respectively. Since $f_2(x)$ is a flipped (with respect to $x$) version of $f_1(x)$, and due to the symmetry of the input-independent Gaussian noise distribution around 0, we have $I_1 = I_2$. Now we consider the mixture of the two distributions $f_3(x) = \tau f_1(x) + (1-\tau) f_2(x)$, $\tau \in [0, 1]$, which has the same support $[0, \mathcal{A}]$ and has mean $\mu_3 = \tau\mu_1 + (1-\tau)\mu_2 \in [\mu_1, \mu_2]$. By Jensen's inequality and the concavity of the mutual information in $f(x)$ for a given $f(y|x)$ [23], we have

$$I(X;Y)|_{f_3(x)} = I_3 \geq \tau I_1 + (1-\tau) I_2 = I_1,$$

with equality if $\tau = 1$ or $\tau = 0$. This means that for any $\mu_1 \leq \frac{\mathcal{A}}{2}$, there exists a distribution with mean $\mu_3 \geq \mu_1$ which achieves higher rate. Similarly for any $\mu_2 \geq \frac{\mathcal{A}}{2}$, there exists a distribution with mean $\mu_3 \leq \mu_2$ which achieves higher rate. Thus, $\mathcal{C}$ is increasing in $\mathbb{E}[X] \in (0, \frac{\mathcal{A}}{2}]$, decreasing in $\mathbb{E}[X] \in (\frac{\mathcal{A}}{2}, \mathcal{A}]$, which proves that the optimal distribution has $\mathbb{E}[X] = \min\{\mathcal{E}, \frac{\mathcal{A}}{2}\}$.

## APPENDIX B
## A GEOMETRIC JUSTIFICATION OF SPHERE-PACKING BOUNDS

In this appendix, we explain why we consider non-overlapping balls while deriving sphere-packing capacity bounds. Note that $P_e^{(n)} \to 0$ as $n \to \infty$ does not necessarily mean that decoding spheres are non-intersecting. One can intuitively say that they might intersect, but this intersection has to be small in some sense.

Next, we show that under $P_e^{(n)} \to 0$ as $n \to \infty$, such an intersection does not change the sphere-packing bound. In particular, we show that if $P_e^{(n)} \to 0$ as $n \to \infty$, then the ratio of the volume of intersection of two spheres $V_i^{(n)}$ to the volume of the sphere $V_s^{(n)}$ also vanishes as $n \to \infty$. Thus $P_e^{(n)} \to 0$ as $n \to \infty$ implies that the volume of the union of the intersecting spheres $V_u^{(n)} \to 2V_s^{(n)}$ as $n \to \infty$. Consequently, spheres with a 'small overlap' behave as non overlapping spheres as $n \to \infty$.

**Error probability lower bound:** Consider a set of codewords $\{\boldsymbol{x}_1, \boldsymbol{x}_2, \cdots, \boldsymbol{x}_{M_n}\}$ where $\boldsymbol{x}_i \in \mathbb{R}^n$, and $M_n$ is the number of codewords. The transmitter chooses one codeword $\boldsymbol{x}_i$ uniformly from this set, and sends this codeword. The receiver receives $\boldsymbol{y} = \boldsymbol{x}_i + \boldsymbol{z}$ where $\boldsymbol{z}$ is i.i.d. Gaussian with zero mean and variance $\sigma^2$. It uses a decoder $g(\boldsymbol{y})$ to recover $\boldsymbol{x}_i$. The probability of error $\lambda_i^{(n)}$ is defined as $\lambda_i^{(n)} = \mathbb{P}\left(g(\boldsymbol{y}) \neq \boldsymbol{x}_i | \boldsymbol{x}_i \text{was sent}\right)$. The maximal probability of error is thus $P_e^{(n)} = \max_{i \in \{1, \cdots, M_n\}} \lambda_i^{(n)}$ [23].[7] Without loss of generality, we focus on $\lambda_1^{(n)}$.

[7]We focus on maximal error probability since a code with a vanishing average error probability can be modified to one with vanishing maximal error probability at essentially the same rate as discussed in [23, p. 204]

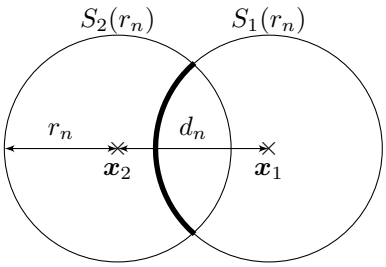


(a) 2 intersecting 2-dimensional spheres (circles) of radius $r_n$ at a distance $d_n$.

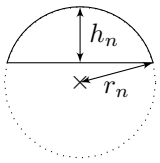


(b) A spherical-cap in 2-dimensions of radius $r_n$ and height $h_n$.

Further, let $g(\boldsymbol{y})$ be a maximum-likelihood (ML) decoder, i.e., it decides in favor of $\boldsymbol{x}_1$ if

$$\mathbb{P}(\boldsymbol{y}|\boldsymbol{x}=\boldsymbol{x}_1) > \mathbb{P}(\boldsymbol{y}|\boldsymbol{x}=\boldsymbol{x}_j),$$

for all $j \in \{2, \cdots, M_n\}$ and in favor of $\boldsymbol{x}_j$ otherwise. This is an optimal decoder. In the Gaussian setting, this rule is equivalent to

$$\|\boldsymbol{y}-\boldsymbol{x}_1\| < \|\boldsymbol{y}-\boldsymbol{x}_j\|,$$

where $\|\cdot\|$ is the $\ell_2$-norm.

As $n \to \infty$, the received signal caused by sending $\boldsymbol{x}_i$ lies almost certainly near the surface of an $n$-dimensional sphere $S_i(r_n)$ of radius $r_n = \sqrt{n\sigma^2}$ about $\boldsymbol{x}_i$. If we send $\boldsymbol{x}_1$, an error will occur if the received $\boldsymbol{y}$ is inside $S_j(r_n)$ for some $j \neq 1$. The probability of error $\lambda_1^{(n)}$ thus coincides with the probability that $\boldsymbol{y}$ lies inside $\bigcup_{j\in\mathcal{J}} S_j(r_n)$, for some $\mathcal{J} \subset \{2, \cdots, M_n\}$ (Fig. 11a shows a graphical illustration). This probability is lower bounded by the probability that $\boldsymbol{y}$ lies in $S_2(r_n)$ (shaded area in Fig. 11a). We focus on this event henceforth, i.e., the event $\{\boldsymbol{y} \in S_2(r_n) | \boldsymbol{x}_1 \text{ was sent}\}$. We denote the probability of this event by $\lambda_{12}^{(n)}$, which satisfies $\lambda_{12}^{(n)} \leq \lambda_1^{(n)}$. We also denote the distance between $\boldsymbol{x}_1$ and $\boldsymbol{x}_2$ by $d_n$, and we restrict ourselves to $d_n \in [0, 2r_n]$, since otherwise, the spheres are disjoint and an error does not occur.

The portion of the surface of $S_1(r_n)$ inside $S_2(r_n)$ is the surface of the spherical-cap $C(r_n, h_n)$ of radius $r_n$ and height $h_n$ as shown in Fig. 11b. The height of this spherical-cap is $h_n = r_n - \frac{d_n}{2}$. By symmetry of the Gaussian distribution, $\boldsymbol{y}$ is uniformly distributed over the surface of $S_1(r_n)$. Therefore, $\lambda_{12}^{(n)}$ can be written as

$$\lambda_{12}^{(n)} = \frac{A(C(r_n, h_n))}{A(S_1(r_n))}, \tag{64}$$

where $A(\cdot)$ is the surface area.[8] The surface area $A(C(r_n, h_n)$ is given by $\frac{1}{2}A(S_1(r_n))I_{\frac{\hat{r}_n^2}{r_n^2}}\left(\frac{n-1}{2}, \frac{1}{2}\right)$ [33], where $\hat{r}_n$ is the radius of the base of the spherical-cap which is $\sqrt{2h_nr_n - h_n^2}$, and $I_x(a,b)$ is the regularized incomplete beta function. Substituting in $\lambda_{12}^{(n)}$, and using $h_n = r_n - \frac{d_n}{2}$, we get

$$\lambda_{12}^{(n)} = \frac{1}{2}I_{1-\frac{d_n^2}{4r_n^2}}\left(\frac{n-1}{2}, \frac{1}{2}\right). \tag{65}$$

[8]We can multiply by $\epsilon_n$ ($\epsilon_n \to 0$ as $n \to \infty$) both in the numerator and denominator to account for the fact that $\boldsymbol{y}$ can be within $\pm\epsilon_n/2$ from the surface of the sphere. But this does not change the result.

In conclusion, we have

$$P_e^{(n)} = \lambda_1^{(n)} \geq \lambda_{12}^{(n)} = \frac{1}{2} I_{1-\frac{d_n^2}{4r_n^2}} \left( \frac{n-1}{2}, \frac{1}{2} \right). \tag{66}$$

**Volume of Intersection:** Now we show that $P_e^{(n)} \to 0$ as $n \to \infty$ implies that $V_i^{(n)}/V_u^{(n)} \to 0$ as $n \to \infty$. First, we note that the intersection of $S_1(r_n)$ and $S_2(r_n)$ is the union of two spherical-caps $C(r_n, h_n)$ of radius $r_n$ and height $h_n = r_n - \frac{d_n}{2}$ (Fig. 11b). Thus

$$V_i^{(n)} = 2V(C(r_n, h_n)), \tag{67}$$

where $V(\cdot)$ is the volume. The volume of such a spherical-cap is given by [33]

$$V(C(r_n, h_n)) = \frac{V(S_1(r_n))}{2} I_{\frac{\hat{r}_n^2}{r_n^2}} \left( \frac{n+1}{2}, \frac{1}{2} \right) \tag{68}$$

$$= \frac{V(S_1(r_n))}{2} I_{1-\frac{d_n^2}{4r_n^2}} \left( \frac{n+1}{2}, \frac{1}{2} \right). \tag{69}$$

Here, $V(S_1(r_n)) = V_s^{(n)}$. Thus,

$$V_i^{(n)} = V_s^{(n)} I_{1-\frac{d_n^2}{4r_n^2}} \left( \frac{n+1}{2}, \frac{1}{2} \right). \tag{70}$$

Therefore,

$$\frac{V_i^{(n)}}{V_s^{(n)}} = I_{1-\frac{d_n^2}{4r_n^2}} \left( \frac{n+1}{2}, \frac{1}{2} \right). \tag{71}$$

Now we use the identity $I_x(a+1, b) = I_x(a, b) - \frac{x^a(1-x)^b}{aB(a,b)}$ for $a > 0$, $b > 0$, and $0 \leq x \leq 1$, where $B(a, b)$ is the beta function [34, 8.17.20]. This identity implies that $I_x(a+1, b) \leq I_x(a, b)$ since $\frac{x^a(1-x)^b}{aB(a,b)} \geq 0$. Therefore, since $1 - \frac{d_n^2}{4r_n^2} \in [0, 1]$, then $\frac{1}{2}\frac{V_i^{(n)}}{V_s^{(n)}} \leq \lambda_{12}^{(n)}$. Combining this inequality with (66) yields

$$P_e^{(n)} = \lambda_1^{(n)} \geq \lambda_{12}^{(n)} \geq \frac{1}{2}\frac{V_i^{(n)}}{V_s^{(n)}} \geq 0. \tag{72}$$

Therefore, $P_e^{(n)} \to 0$ as $n \to \infty$ implies $\frac{V_i^{(n)}}{V_s^{(n)}} \to 0$ as $n \to \infty$. Consequently, for vanishing error probability, $V_u^{(n)} = 2V_s^{(n)} - V_i^{(n)} \to 2V_s^{(n)}$ as $n \to \infty$.

We conclude that the union of two 'slightly overlapping' spheres behaves (in terms of volume) as two non-overlapping spheres as $n \to \infty$. We finally note that these arguments can be applied for any two codewords $\boldsymbol{x}_i$ and $\boldsymbol{x}_j$ provided that $P_e^{(n)} \to 0$ as $n \to \infty$. In this case, all intersections are relatively vanishing (with respect to $V_s^{(n)}$) as $n \to \infty$. Thus, even if there is a small overlap in the spheres, the sphere packing bound would provide the same number of spheres as if spheres are non-overlapping, in the limit as $n \to \infty$. This explains why sphere-packing bounds can provide capacity upper bounds.

## APPENDIX C
## BOUNDING THE LIMIT IN (7)

We need to upper bound the limit $\lim_{n\to\infty} \frac{1}{n} \log\left(\sum_{i=0}^{n} N_i\right)$ where $N_i = \binom{n}{n-i} \left(\frac{\mathcal{A}}{\sqrt{\pi n \sigma^2}}\right)^{n-i} \frac{\Gamma\left(1+\frac{n}{2}\right)}{\Gamma\left(1+\frac{i}{2}\right)}$. To this end, we start by writing $N_i$ as

$$N_i = \left(\frac{\mathcal{A}}{\sqrt{\pi n \sigma^2}}\right)^{n-i} \frac{\Gamma\left(1+\frac{n}{2}\right)\Gamma\left(1+n\right)}{\Gamma\left(1+\frac{i}{2}\right)\Gamma\left(1+n-i\right)\Gamma\left(1+i\right)} \tag{73}$$

using the definition of the binomial coefficient and the Gamma function [35]. Note that

$$\frac{1}{n}\log\left(\sup_{i\in\{0,\cdots,n\}} N_i\right) \leq \frac{1}{n}\log\left(\sum_{i=0}^{n} N_i\right) \leq \frac{1}{n}\log\left((n+1)\sup_{i\in\{0,\cdots,n\}} N_i\right)$$

and that

$$\lim_{n\to\infty}\frac{1}{n}\log\left(\sup_{i\in\{0,\cdots,n\}} N_i\right) = \lim_{n\to\infty}\frac{1}{n}\log\left((n+1)\sup_{i\in\{0,\cdots,n\}} N_i\right).$$

Thus

$$\lim_{n\to\infty}\frac{1}{n}\log\left(\sum_{i=0}^{n} N_i\right) = \lim_{n\to\infty}\frac{1}{n}\log\left(\sup_{i\in\{0,\cdots,n\}} N_i\right) \tag{74}$$

$$= \lim_{n\to\infty}\sup_{i\in\{0,\cdots,n\}}\frac{1}{n}\log\left(N_i\right) \tag{75}$$

where the second step follows by the monotonicity of the logarithm. Now we relax this expression by replacing $i \in \{0,\cdots,n\}$ by $\alpha n$ with $\alpha \in [0,1]$. This leads to

$$\lim_{n\to\infty}\frac{1}{n}\log\left(\sum_{i=0}^{n} N_i\right) \leq \lim_{n\to\infty}\sup_{\alpha\in[0,1]}\frac{1}{n}\log\left(N_{\alpha n}\right). \tag{76}$$

Using Stirling's bound [36] $\sqrt{2\pi}n^{n+\frac{1}{2}}e^{-n} \leq \Gamma(n) \leq n^{n+\frac{1}{2}}e^{1-n}$, we obtain

$$N_{\alpha n} \leq \left[\left(\frac{\mathcal{A}^2}{2\pi e\sigma^2}\right)^{\frac{1-\alpha}{2}}\alpha^{-\frac{3\alpha}{2}}(1-\alpha)^{\alpha-1}\right]^n \frac{e^2}{2\pi\sqrt{2\pi}\alpha n\sqrt{1-\alpha}}. \tag{77}$$

Therefore, the limit $\lim_{n\to\infty}\frac{1}{n}\log\left(N_{\alpha n}\right)$ exists, and is equal to

$$B_1'(\alpha) = (1-\alpha)\log\left(\frac{\gamma}{\sqrt{2\pi e}}\right) - \log\left((1-\alpha)^{1-\alpha}\alpha^{\frac{3\alpha}{2}}\right).$$

Since the limit exists, we can exchange the $\lim$ and the $\sup$ leading to

$$\lim_{n\to\infty}\frac{1}{n}\log\left(\sum_{i=0}^{n} N_i\right) \leq \sup_{\alpha\in[0,1]} B_1'(\alpha). \tag{78}$$

Now by replacing $\alpha$ by $1-\alpha$, we obtain $B_1(\alpha)$ and the the upper bound $\overline{\mathcal{C}}_{\mathcal{A},1}$ given in Theorem 1.

## APPENDIX D
## BOUNDING THE EQUIVALENT HEIGHT OF A SPHERICAL-CAP

The volume of a spherical-cap of radius $\lambda$ and height $h \in [0,\lambda]$ is [33]

$$V(\mathcal{P}_{\lambda,h}^n) = \frac{1}{2}V(\mathcal{B}_\lambda^n)I_{\frac{\lambda'^2}{\lambda^2}}\left(\frac{n+1}{2},\frac{1}{2}\right), \tag{79}$$

where $\lambda' = \sqrt{2h\lambda - h^2}$. The base of this spherical-cap is $\mathcal{B}_{\lambda'}^{n-1}$. Thus, the height of the equivalent cylinder is

$$h' = \frac{1}{2}\frac{V(\mathcal{B}_\lambda^n)}{V(\mathcal{B}_{\lambda'}^{n-1})}I_{\frac{\lambda'^2}{\lambda^2}}\left(\frac{n+1}{2},\frac{1}{2}\right) \tag{80}$$

$$= \hat{h}_n\frac{V(\mathcal{B}_\lambda^{n-1})}{V(\mathcal{B}_{\lambda'}^{n-1})}I_{\frac{\lambda'^2}{\lambda^2}}\left(\frac{n+1}{2},\frac{1}{2}\right), \tag{81}$$

where $\hat{h}_n = \frac{V(\mathcal{B}_\lambda^n)}{2V(\mathcal{B}_\lambda^{n-1})}$. Thus,

$$h' = \hat{h}_n\left(\frac{\lambda^2}{\lambda'^2}\right)^{\frac{n-1}{2}}I_{\frac{\lambda'^2}{\lambda^2}}\left(\frac{n+1}{2},\frac{1}{2}\right). \tag{82}$$

Using the identity $I_x(a,b) = \frac{a^{-1}x^a F(a,1-b;a+1;x)}{a^{-1}F(a,1-b;a+1;1)}$ [35, Sec. 6.6] where $F(a,b;c;x)$ is the Gauss hypergeometric function, we can write

$$h' = \hat{h}_n \left(\frac{\lambda^2}{\lambda'^2}\right)^{\frac{n-1}{2}} \frac{\left(\frac{\lambda'^2}{\lambda^2}\right)^{\frac{n+1}{2}} F\left(\frac{n+1}{2}, \frac{1}{2}; \frac{n+3}{2}; \frac{\lambda'^2}{\lambda^2}\right)}{F\left(\frac{n+1}{2}, \frac{1}{2}; \frac{n+3}{2}; 1\right)} \tag{83}$$

$$= \hat{h}_n \underbrace{\left(\frac{\lambda'^2}{\lambda^2}\right) \frac{F\left(\frac{n+1}{2}, \frac{1}{2}; \frac{n+3}{2}; \frac{\lambda'^2}{\lambda^2}\right)}{F\left(\frac{n+1}{2}, \frac{1}{2}; \frac{n+3}{2}; 1\right)}}_{f(\lambda')}. \tag{84}$$

But since $h \in [0,\lambda]$, then $\lambda' \in [0,\lambda]$. Furthermore, both $\frac{\lambda'^2}{\lambda^2}$ and $F\left(\frac{n+1}{2}, \frac{1}{2}; \frac{n+3}{2}; \frac{\lambda'^2}{\lambda^2}\right)$ are increasing functions of $\lambda'$, and hence, $f(\lambda')$ is increasing in $\lambda'$. Since $f(0) = 0$ and $f(\lambda) = 1$, we conclude that $h' \leq \hat{h}_n$.

## APPENDIX E
## DERIVATION OF THE LOWER BOUND IN SECTION VI-B

We start by writing the achievable rate $R = I(X;Y)$ with input distribution $\tilde{g}_{\mu_0,\sigma_0}(x)$ described in (30) as

$$\mathcal{R} = \int_0^{\mathcal{A}} \int_{-\infty}^{\infty} f(x,y) \log\left(\frac{f(y|x)}{f(y)}\right) dydx \tag{85}$$

$$= \int_0^{\mathcal{A}} \int_{-\infty}^{\infty} f(x,y) \log\left(f(y|x)\right) dydx - \int_0^{\mathcal{A}} \int_{-\infty}^{\infty} f(x,y) \log\left(f(y)\right) dydx. \tag{86}$$

The first integral above is $-h(Z)$ ($h(Z)$ is the entropy of noise), and hence

$$\int_0^{\mathcal{A}} \int_{-\infty}^{\infty} f(x,y) \log\left(f(y|x)\right) dydx = -\frac{1}{2}\log(2\pi e\sigma^2). \tag{87}$$

Next, we substitute $f(y) = \eta g_{\mu_0,\sigma_y}(y)(G_{\mu',\nu'}(\mathcal{A}) - G_{\mu',\nu'}(0))$ in the second integral to obtain

$$T = \int_0^{\mathcal{A}} \int_{-\infty}^{\infty} f(x,y) \log\left(\eta\right) dydx + \int_0^{\mathcal{A}} \int_{-\infty}^{\infty} f(x,y) \log\left(g_{\mu_0,\sigma_y}(y)\right) dydx \tag{88}$$

$$+ \int_0^{\mathcal{A}} \int_{-\infty}^{\infty} f(x,y) \log\left(G_{\mu',\nu'}(\mathcal{A}) - G_{\mu',\nu'}(0)\right) dydx$$

$$= T_1 + T_2 + T_3, \tag{89}$$

where $T_1$, $T_2$, and $T_3$ denote the first, second, and third integrals above, respectively. The first term $T_1$ is clearly

$$T_1 = \log(\eta). \tag{90}$$

The last term $T_3$ can be written as

$$T_3 = \mathbb{E}_{X,Y}[\log\left(G_{\mu',\nu'}(\mathcal{A}) - G_{\mu',\nu'}(0)\right)] \tag{91}$$

where the expectation is with respect to the distribution $f(x,y)$. It remains to evaluate $T_2$ in order to obtain the achievable rate $\mathcal{R}$ in Theorem 4. We start by substituting $g_{\mu,\sigma_y}(y)$ in $T_2$, yielding

$$T_2 = \int_0^{\mathcal{A}} \int_{-\infty}^{\infty} f(x,y) \log\left(\sqrt{\frac{1}{2\pi\sigma_y^2}}\right) dydx + \int_0^{\mathcal{A}} \int_{-\infty}^{\infty} f(x,y) \left(-\frac{(y-\mu)^2}{2\sigma_y^2}\right) dydx \tag{92}$$

$$= -\frac{1}{2}\log\left(2\pi\sigma_y^2\right) - \frac{1}{2\sigma_y^2}\int_0^{\mathcal{A}} \left(\mathbb{E}_{Y|X}\left[Y^2\right] - 2\mu\mathbb{E}_{Y|X}\left[Y\right] + \mu^2\right)\tilde{g}_{\mu,\nu}(x)dx \tag{93}$$

$$= -\frac{1}{2}\log\left(2\pi\sigma_y^2\right) - \frac{1}{2\sigma_y^2}\int_0^{\mathcal{A}} \left(\sigma^2 + (x-\mu)^2\right)\tilde{g}_{\mu,\nu}(x)dx \tag{94}$$

$$= -\frac{1}{2}\log\left(2\pi\sigma_y^2\right) - \frac{1}{2\sigma_y^2}\left(\sigma^2 + \mathbb{E}_X[(X-\mu)^2]\right). \tag{95}$$

Finally, we need to evaluate the expectation $\mathbb{E}_X[(X-\mu)^2]$. To this end, we use a change of variables, followed by the identity

$$\int_a^b t^2 e^{-t^2} dt = \frac{1}{2}\left(\int_a^b e^{-t^2}dt - \left[te^{-t^2}\right]_a^b\right), \tag{96}$$

to get

$$\mathbb{E}_X[(X-\mu)^2] = \eta\frac{2\nu^2}{\sqrt{\pi}}\int_{-\frac{\mu}{\sqrt{2}\nu}}^{\frac{\mathcal{A}-\mu}{\sqrt{2}\nu}} t^2 e^{-t^2} dt \tag{97}$$

$$= \eta\frac{\nu^2}{\sqrt{\pi}}\left(\int_{-\frac{\mu}{\sqrt{2}\nu}}^{\frac{\mathcal{A}-\mu}{\sqrt{2}\nu}} e^{-t^2}dt - \left[te^{-t^2}\right]_{-\frac{\mu}{\sqrt{2}\nu}}^{\frac{\mathcal{A}-\mu}{\sqrt{2}\nu}}\right) \tag{98}$$

$$= \nu^2\left[\int_0^{\mathcal{A}} \tilde{g}_{\mu,\nu}(x)dx - (\mathcal{A}-\mu)\tilde{g}_{\mu,\nu}(\mathcal{A}) - \mu\tilde{g}_{\mu,\nu}(0)\right] \tag{99}$$

$$= \nu^2\left(1 - (\mathcal{A}-\mu)\tilde{g}_{\mu,\nu}(\mathcal{A}) - \mu\tilde{g}_{\mu,\nu}(0)\right). \tag{100}$$

Collecting all terms (87), (89)-(91), (95), and (100), and substituting in (86), yields the desired expression

$$\mathcal{R} = \frac{1}{2}\log\left(1+\frac{\nu^2}{\sigma^2}\right) - \log(\eta) - \left((\mathcal{A}-\mu)\tilde{g}_{\mu,\nu}(\mathcal{A}) + \mu\tilde{g}_{\mu,\nu}(0)\right)\frac{\nu^2}{2(\nu^2+\sigma^2)} - \mathbb{E}_{X,Y}\left[\log(G_{\mu',\nu'}(\mathcal{A}) - G_{\mu',\nu'}(0))\right],$$

where we replaced $\sigma_y^2$ by its value $\sigma^2+\nu^2$. This completes the proof of the achievable rate $\mathcal{R}$ in Theorem 4.

Note that since $\eta > 1$, then $T_1 = \log(\eta)$ can be considered as a penalty term arising due to the truncation of the Gaussian distribution, which reduces the rate below $\frac{1}{2}\log\left(1+\frac{\nu^2}{\sigma^2}\right)$. The second term $T_2$ can be positive or negative depending on the choice of $\mu$ and $\nu$. If $\mu$ is positive, then this term is clearly positive, and is hence also a penalty term. If $\mu$ is negative, the second term can be negative and increases the achievable rate. The last term $T_3$ is always negative, and hence it always increases the achievable rate. Since this term might be difficult to compute, and since it is always negative, we can drop it an obtain the achievable rate $\mathcal{R}'$ as given in Theorem 4.

## APPENDIX F
## GAP BETWEEN $\mathcal{R}'$ AND SPHERE-PACKING BOUNDS FOR SELECTIONS OF $\mu$ AND $\nu$

Recall that the achievable rate $\mathcal{R}'$ is given by

$$\mathcal{R}' = \frac{1}{2}\log\left(1+\frac{\nu^2}{\sigma^2}\right) - \log(\eta) - \left((\mathcal{A}-\mu)g_{\mu,\nu}(\mathcal{A}) + \mu g_{\mu,\nu}(0)\right)\frac{\eta\nu^2}{2(\nu^2+\sigma^2)},$$

where $\eta = \frac{1}{G_{\mu,\nu}(\mathcal{A}) - G_{\mu,\nu}(0)}$, and where $\mu$ and $\nu$ are chosen such that

$$\tilde{\mu} = \nu^2 \eta (g_{\mu,\nu}(0) - g_{\mu,\nu}(\mathcal{A})) + \mu \leq \mathcal{E}.$$

Now let us fix $\mu = 0$ and $\nu = \sqrt{\frac{\pi}{2}}\mathcal{E}$. To simplify the computation, we would like to have $G_{\mu,\nu}(\mathcal{A}) \approx 1$, which can be achieved if $\nu \leq \frac{\mathcal{A}}{3}$ leading to the constraint $\mathcal{E} \leq \frac{\mathcal{A}}{3}\sqrt{\frac{2}{\pi}}$. Using this selection for $\mathcal{E} \in \left(0, \frac{\mathcal{A}}{3}\sqrt{\frac{2}{\pi}}\right]$, we have $G_{\mu,\nu}(\mathcal{A}) \approx 1$, $G_{\mu,\nu}(0) = \frac{1}{2}$, $g_{\mu,\nu}(\mathcal{A}) < \frac{1}{\pi\mathcal{E}} e^{-\frac{\mathcal{A}^2}{\pi\mathcal{E}^2}}$, $g_{\mu,\nu}(0) = \frac{1}{\pi\mathcal{E}}$. This selection leads to $\eta \approx 2$ and $\tilde{\mu} < \mathcal{E}$. The achievable rate is given by

$$\mathcal{R}' = \frac{1}{2}\log\left(1 + \frac{\pi\mathcal{E}^2}{2\sigma^2}\right) - \log(2) - \mathcal{A} g_{\mu,\nu}(\mathcal{A}) \frac{\nu^2}{\nu^2 + \sigma^2} \tag{101}$$

$$> \frac{1}{2}\log\left(\frac{\pi\mathcal{E}^2}{8\sigma^2}\right) - \mathcal{A} g_{\mu,\nu}(\mathcal{A}). \tag{102}$$

But $\mathcal{A} g_{\mu,\nu}(\mathcal{A}) < \frac{\mathcal{A}}{\pi\mathcal{E}} e^{-\frac{\mathcal{A}^2}{\pi\mathcal{E}^2}} = \frac{1}{\sqrt{\pi}} t e^{-t^2}$ where $t = \frac{\mathcal{A}}{\sqrt{\pi}\mathcal{E}}$. But for $\mathcal{E} \leq \frac{\mathcal{A}}{3}\sqrt{\frac{2}{\pi}}$, $t > \frac{3}{\sqrt{2}} > \frac{1}{\sqrt{2}}$. Since the function $te^{-t^2}$ is decreasing for $t > \frac{1}{\sqrt{2}}$, then $\mathcal{A} g_{\mu,\nu}(\mathcal{A}) < \frac{1}{\sqrt{\pi}} \frac{3}{\sqrt{2}} e^{-\frac{9}{2}} < 0.0133$.

Therefore, at high SNR where the sphere packing bound $\overline{\mathcal{C}}_{\mathcal{E}}$ becomes $\frac{1}{2}\log\left(\frac{e\mathcal{E}^2}{2\pi\sigma^2}\right)$ the gap can be bounded as

$$\overline{\mathcal{C}}_{\mathcal{E}} - \mathcal{R}' < \frac{1}{2}\log\left(\frac{e}{2\pi}\frac{8}{\pi}\right) + 0.0133$$

$$< 0.062.$$

Similar analysis can be applied to all other cases leading to the values given in Table II.

## REFERENCES


[1] J. Akella, M. Yuksel, and S. Kalyanaraman, "Error analysis of multi-hop free-space optical communications," in *Proc. of IEEE International Conference on Communications (ICC)*, May. 2005, pp. 1777–1781.

[2] S. Kazemlou, S. Hranilovic, and S. Kumar, "All-optical multihop free-space optical communication systems," *Journal of Lightwave Technology*, vol. 29, no. 18, pp. 2663–2669, Jun. 2011.

[3] E. Zedini, I. S. Ansari, and M.-S. Alouini, "Performance analysis of mixed Nakagami-m and Gamma-Gamma dual-hop FSO transmission systems," *IEEE Photonics Journal*, vol. 7, no. 1, Dec. 2014.

[4] Q. Gao, R. Wang, Z. Xu, and Y. Hua, "DC-informative joint color-frequency modulation for visible light communications," *Journal of Lightwave Technology*, vol. 33, no. 11, pp. 2181–2188, June 2015.

[5] H. Elgala, R. Mesleh, and H. Haas, "Indoor optical wireless communication: Potential and state-of-the-art," *IEEE Comm. Magazine*, vol. 49, no. 9, pp. 56–62, Sep. 2011.

[6] A. García-Zambrana, C. Castillo-Vázquez, and B. Castillo-Vázquez, "On the capacity of FSO links over Gamma-Gamma atmospheric turbulence channels using OOK signaling," *EURASIP J. Wirel. Commun. Netw.*, Jan. 2010.

[7] S. Arnon, J. Barry, G. Karagiannidis, R. Schober, and M. Uysal, *Advanced Optical Wireless Communication Systems*. Cambridge University Press, 2012.

[8] M. A. Khalighi and M. Uysal, "Survey on free space optical communications: A communication theory perspective," *IEEE Communication Surveys and Tutorials*, vol. 16, no. 4, pp. 2231–2258, 4th quarter 2014.

[9] A. Lapidoth, S. M. Moser, and M. Wigger, "On the capacity of free-space optical intensity channels," *IEEE Trans. on Info. Theory*, vol. 55, no. 10, pp. 4449–4461, Oct. 2009.

[10] A. A. Farid and S. Hranilovic, "Channel capacity and non-uniform signalling for free-space optical intensity channels," *IEEE Journal on Selected Areas in Communications*, vol. 27, no. 9, pp. 1–12, Dec. 2009.

[11] ——, "Capacity bounds for wireless optical intensity channels with Gaussian noise," *IEEE Trans. on Info. Theory*, vol. 56, no. 12, pp. 6066–6077, Dec. 2010.

[12] ——, "Outage capacity optimization for free-space optical links with pointing errors," *IEEE/OSA Journal of Lightwave Technology*, vol. 25, no. 7, pp. 1702–1710, Jul. 2007.

[13] O. E. DeLange, "Optical heterodyne detection," *IEEE Spectrum*, vol. 5, no. 10, pp. 77–85, Oct. 1968.

[14] T. H. Chan, S. Hranilovic, and F. R. Kschischang, "Capacity-achieving probability measure for conditionally Gaussian channel with bounded input," *IEEE Trans. on Info. Theory*, vol. 51, no. 6, pp. 2073–2088, Jun. 2005.

[15] S. V. Kartalopoulos, *Free Space Optical Networks for Ultra-Broad Band Services*. John Wiley and Sons, Inc., 2011.

[16] S. M. Moser, "Capacity results of an optical intensity channel with input-dependent Gaussian noise," *IEEE Trans. on Info. Theory*, vol. 58, no. 1, pp. 207–223, Jan. 2012.

[17] M. Berger, *Geometry II*. Springer-Verlag, 1987.

[18] J. M. Morvan, *Generalized Curvatures*. Springer-Verlag, 2008.

[19] D. Cohen-Steiner and J. M. Morvan, "Restricted Delaunay triangulations and normal cycle," in *Proceedings of the Nineteenth Annual Symposium on Computational Geometry (SoCG), A.C.M. Press, New York, NY, USA*, 2003, pp. 312–321.

[20] H. Kazemi, Z. Mostaani, M. Uysal, and Z. Ghassemlooy, "Outage performance of MIMO FSO systems in Gamma-Gamma fading channels," in *Proc. of IEEE 18th European Conference on Network and Optical Communications*, Graz, Austria, Jul. 2013.

[21] M. A. Kashani and M. Uysal, "Outage performance and diversity gain analysis of free-space optical multi-hop parallel relaying," *IEEE/OSA Journal of Optical Communications and Networking*, vol. 5, no. 8, pp. 901–909, Aug. 2013.

[22] A. A. Farid and S. Hranilovic, "Diversity gain and outage probability for MIMO free-space optical links with misalignment," *IEEE Trans. on Communications*, vol. 60, no. 2, pp. 479–487, Feb. 2012.

[23] T. Cover and J. Thomas, *Elements of Information Theory (Second Edition)*. John Wiley and Sons, Inc., 2006.

[24] H. AlQuwaiee, I. S. Ansari, and M.-S. Alouini, "On the performance of free-space optical communication systems over double generalized Gamma channel," *IEEE Journal on Selected Areas in Communications*, May 2015.

[25] C. E. Shannon, "Communication in the presence of noise," *Proceedings of the IRE*, vol. 37, no. 1, pp. 10–21, Jan. 1949.

[26] S. Rabinowitz, "The volume of an n-simplex with many equal edges," *Missouri Journal of Mathematical Sciences*, vol. 1, pp. 11–17, 1989.

[27] D. Tse and P. Viswanath, *Fundamentals of Wireless Communications*. Cambridge University Press, 2005.

[28] M. K. Simon and M.-S. Alouini, *Digital Communication over Fading Channels*. John Wiley and Sons, Inc., 2005.

[29] B. M. Oliver, "Thermal and quantum noises," in *Proc. of the IEEE*, vol. 53, May 1965, pp. 436–454.

[30] S. Shamai (Shitz) and I. Bar-David, "The capacity of average and peak-power-limited quadrature Gaussian channels," *IEEE Trans. on Info. Theory*, vol. 41, no. 4, pp. 1060–1071, Jul. 1995.

[31] C. E. Shannon, "A mathematical theory of communication," *The Bell System Technical Journal*, vol. 27, pp. 379–423, 623–656, 1948.

[32] J. A. Thomas, "Feedback can at most double Gaussian multiple access channel capacity," *IEEE Trans. on Info. Theory*, vol. 33, no. 5, pp. 711–716, Sep. 1987.

[33] S. Li, "Concise formulas for the area and volume of a hyperspherical cap," *Asian Journal of Mathematics and Statistics*, vol. 4, pp. 66–70, Nov. 2010.

[34] F. W. J. Olver, D. W. Lozier, R. F. Boisvert, and C. W. Clark, Eds., *NIST Handbook of Mathematical Functions*. New York, NY: Cambridge University Press, 2010, print companion to [**?**].

[35] M. Abramowitz and I. A. Stegun, *Handbook of Mathematical Functions*. Dover Publications, 1964.

[36] W. Feller, *An Introduction to Probability Theory and its Applications (3rd Edition)*. Wiley, 1968, vol. 1.